Competing isomeric product channels in the 193 nm photodissociation of 2-chloropropene and in the unimolecular dissociation of the 2-propenyl radical

Julie A. Mueller, Bradley F. Parsons, and Laurie J. Butler[a)]
The James Franck Institute and Department of Chemistry, University of Chicago, Chicago, Illinois 60637

Fei Qi, Osman Sorkhabi, and Arthur G. Suits
Chemical Sciences Division, Lawrence Berkeley National Laboratory, Berkeley, California 94720

(Received 10 August 2000; accepted 13 December 2000)

This paper presents product translational energy spectroscopy measurements of the primary photofragmentation channels of 2-chloropropene excited at 193 nm and of the unimolecular dissociation of the 2-propenyl radical. Tunable vacuum ultraviolet (VUV) photoionization of the products allows us to distinguish between the various product isomers formed in these processes. The data show evidence for three significant primary reaction channels in the dissociation of 2-chloropropene: An excited-state C–Cl fission channel producing fast Cl atoms, a C–Cl fission channel producing slow Cl atoms, and HCl elimination. A minor $C-CH_3$ fission channel contributes as well. The measured branching of the major primary product channels is: [fast C–Cl]:[slow C–Cl]:[HCl elimination] = 62%:23%:15%. The experiments also allow us to resolve selectively the product branching between the unimolecular dissociation channels of the 2-propenyl radical, a high energy C_3H_5 isomer; we measure how the branching ratio between the two competing C–H fission channels changes as a function of the radical's internal energy. The data resolve the competition between the unimolecular H+allene and H+propyne product channels from the radical with internal energies from 0 to 18 kcal/mol above the H+propyne barrier. We find that the barrier to H+allene formation from this high-energy C_3H_5 radical is higher than the barrier to H+propyne formation, in agreement with recent theoretical calculations but in sharp contrast to that predicted for the most stable C_3H_5 isomer, the allyl radical. The experiments demonstrate a general technique for selectively forming a particular C_nH_m isomer dispersed by internal energy due to the primary photolysis, thus allowing us to determine the branching between unimolecular dissociation channels as a function of the selected radical isomer's internal energy. © *2001 American Institute of Physics.* [DOI: 10.1063/1.1345877]

I. INTRODUCTION

One of the most basic goals of chemistry is to determine the products of chemical reactions when several pathways are possible. This goal is often difficult to achieve when products include more than one isomer of the same species or when short-lived radicals are involved as either reactants or products. The 193 nm photodissociation of 2-chloropropene ($H_2CCClCH_3$) first provides the opportunity to investigate the competition between bond fission and molecular elimination product channels occurring in competition on both the ground electronic state and excited electronic potential-energy surfaces. More importantly, the experimental method presented here also allows us to study the competing C–H bond fission processes of the 2-propenyl radical, a C_3H_5 radical isomer 19.4 kcal/mol higher in energy[1] than the allyl radical, with the radicals dispersed by internal energy in the primary photolysis. The isomerization and unimolecular dissociation of this radical has received considerable attention in studies where it was embedded in C_3H_5 kinetics[1–3] or allyl radical dynamics[4–6] studies. The method presented here opens up the study of the unimolecular dissociation processes of a wide range of normally elusive isomeric radical species.

Despite its common use in organic synthesis and its well-characterized infrared (IR) spectroscopy,[7–9] we found no UV-vis absorption spectra of 2-chloropropene in the literature. However, because of the molecule's structural similarity to the better-characterized vinyl chloride, we expect a strong absorption band in the region of 193 nm to excite a primarily $\pi\pi^*$ transition. This paper reports the UV absorption spectrum from 300 to 190 nm, *ab initio* calculations of the low-lying excited electronic states of 2-chloropropene, and the emission spectrum from the molecule excited at 199.7 nm; those data confirm our expectation that absorption at 193 nm excites a $\pi\pi^*$ transition analogous to that in vinyl chloride.

A rather large number of dissociation and elimination reactions are open to 2-chloropropene excited by a 193 nm photon. In addition to the obvious primary reactions, it is possible for many of the primary products to have sufficient internal energy to undergo secondary dissociation reactions. In the following list of energetically allowed reactions, secondary dissociation reactions are shown as indented and only some are given:

a)Electronic mail: l-butler@uchicago.edu

$$H_2C{=}CClCH_3 \rightarrow H_2C{=}C^*Cl + CH_3, \quad \Delta H \approx 101.6 \text{ kcal/mol},^{10,11} \quad (1)$$

$$H_2C{=}C^*Cl \rightarrow C_2H_2 + Cl, \quad \Delta H \approx 22.6 \text{ kcal/mol},^{1,12} \quad (2)$$

$$H_2C{=}CClCH_3 \rightarrow H_2C{=}C^*CH_3 + Cl, \quad \Delta H_0 \approx 93.4 \text{ kcal/mol},^{13} \quad (3)$$

$$H_2C{=}C^*CH_3 \rightarrow H_2C{=}C{=}CH_2(\text{allene}) + H, \quad \Delta H_0 = 35.0 \text{ kcal/mol},^{1} \quad (4)$$

$$H_2C{=}C^*CH_3 \rightarrow HC{\equiv}CCH_3(\text{propyne}) + H, \quad \Delta H_0 = 33.9 \text{ kcal/mol},^{1} \quad (5)$$

$$H_2C{=}CClCH_3 \rightarrow H_2C{=}C{=}CH_2(\text{allene}) + HCl, \quad \Delta H_0 = 26.1 \text{ kcal/mol},^{14,15} \quad (6)$$

$$H_2C{=}C{=}CH_2 \rightarrow HCCCH_2(\text{propargyl}) + H, \quad \Delta H_0 = 87.8 \text{ kcal/mol},^{16} \quad (7)$$

$$H_2C{=}CClCH_3 \rightarrow HC{\equiv}CCH_3(\text{propyne}) + HCl, \quad \Delta H_0 = 25.0 \text{ kcal/mol},^{17} \quad (8)$$

$$HC{\equiv}CCH_3 \rightarrow HCCCH_2(\text{propargyl}) + H, \quad \Delta H_0 = 88.7 \text{ kcal/mol},^{15} \quad (9)$$

$$H_2C{=}CClCH_3 \rightarrow HCCClCH_3 + H, \quad \Delta H \approx 109 \text{ kcal/mol},^{10,18} \quad (10)$$

$$H_2C{=}CClCH_3 \rightarrow H_2CCClCH_2 + H, \quad (11)$$

$$H_2C{=}CClCH_3 \rightarrow CCClCH_3 + H_2, \quad \Delta H \approx 91 \text{ kcal/mol},^{10,16} \quad (12)$$

$$H_2C{=}CClCH_3 \rightarrow H_2CCClCH + H_2. \quad (13)$$

Elimination of HCl from 2-chloropropene can result in the production of either allene ($H_2C{=}C{=}CH_2$) or propyne ($HC{\equiv}CCH_3$), as indicated in reactions (6) and (8). If the elimination takes place across the double bond, forming propyne, it may be useful to compare the result of the 2-chloropropene elimination reaction with HCl elimination in vinyl chloride. In the latter molecule, both 1, 1 and 1, 2 (i.e., 3-center and 4-center) eliminations are possible. Previous work on vinyl chloride[10,19] has led to the proposal[23,25] that the HCl elimination takes place via a 1, 1 mechanism, although the evidence is not conclusive. Since allene and propyne have different ionization potentials,[15] it is in principle possible to distinguish which products are formed in the 2-chloropropene HCl elimination by measuring the ionization onset of the mass 40 photoproduct. A difficulty exists, however, because the barrier to isomerization from propyne to allene

$$HC{\equiv}CCH_3 \rightarrow H_2C{=}C{=}CH_2, \quad (14)$$

is only about 65 kcal/mol.[1,27] The maximum energy available to the propyne products formed in HCl elimination is over 120 kcal/mol, thus the mass 40 products are susceptible to secondary C–H bond fission as well as isomerization.

There are two particularly interesting pairs of competing product channels, the HCl elimination reactions (6) and (8) in the dissociation of the 2-chloropropene parent and the C–H bond fission reactions (4) and (5) in the secondary dissociation of the 2-propenyl radical. The calculated energetics of each transition state are shown in Fig. 1. The barrier to the HCl elimination forming allene (6) is nearly identical to the one for HCl elimination forming propyne (8).[30] *Ab initio* calculations by Davis *et al.*[1] to determine the barriers to hydrogen atom loss from the 2-propenyl radical to give the isomers allene and propyne [(4) and (5), respectively] show these barriers to be very similar as well. Their results, obtained at the G2(B3LYP) level of theory,[1] give values of 37.1 kcal/mol for the barrier (zero-point corrected) to dissociation yielding propyne, and 38.1 kcal/mol for the reaction yielding allene. Thus, assuming ground-state reactions, the branching between the two HCl elimination reactions and between the two C–H fission reactions is largely controlled by the tightness of the transition state,[31] providing a particularly clear example of the importance of freezing internal rotors in controlling the rate of a chemical reaction.

In this work, after reporting the UV absorption spectrum of 2-chloropropene and the emission from the molecule excited in the $\pi\pi^*$ absorption band, we focus attention on determining the competition between the primary dissociation reactions of 2-chloropropene and the secondary dissociation channels of the nascent 2-propenyl radical products. We use the experimental method of photofragment translational energy spectroscopy, measuring the photoproduct velocity distributions in a crossed laser-molecular beam apparatus, but employing the scattering apparatus at the Advanced Light Source in Berkeley[32] to allow us to use tunable photoionization detection of the products. In this way we can not only distinguish between allene and propyne products (which have different ionization energies),[15] but we can use the products' neutral time-of-flight to determine which came from primary HCl elimination and which came from secondary C–H fission from the primary 2-propenyl product of reaction (3). The experiments also provide one more exciting piece of information not previously revealed in any experiment, but reported in a preliminary communication of this work.[33] Because the primary C–Cl bond fission channel produces the high-energy 2-propenyl radical (an isomer 19.4 kcal/mole higher in energy[1] than the most stable C_3H_5 radical isomer, the allyl radical) with neutral product recoil velocities which identify the internal energy of the nascent radical, the radicals are effectively dispersed by their internal energy. Then because C–H fission from the radicals formed with enough internal energy to dissociate produces mass 40 products travelling with essentially the same velocity as their 2-propenyl parents, the arrival time of the mass 40 product identifies the internal energy of the radical from which it came! Thus, we can measure how the branching between the H+allene (4) and the H+propyne (5) product channels from the unimolecular dissociation of the 2-propenyl radicals

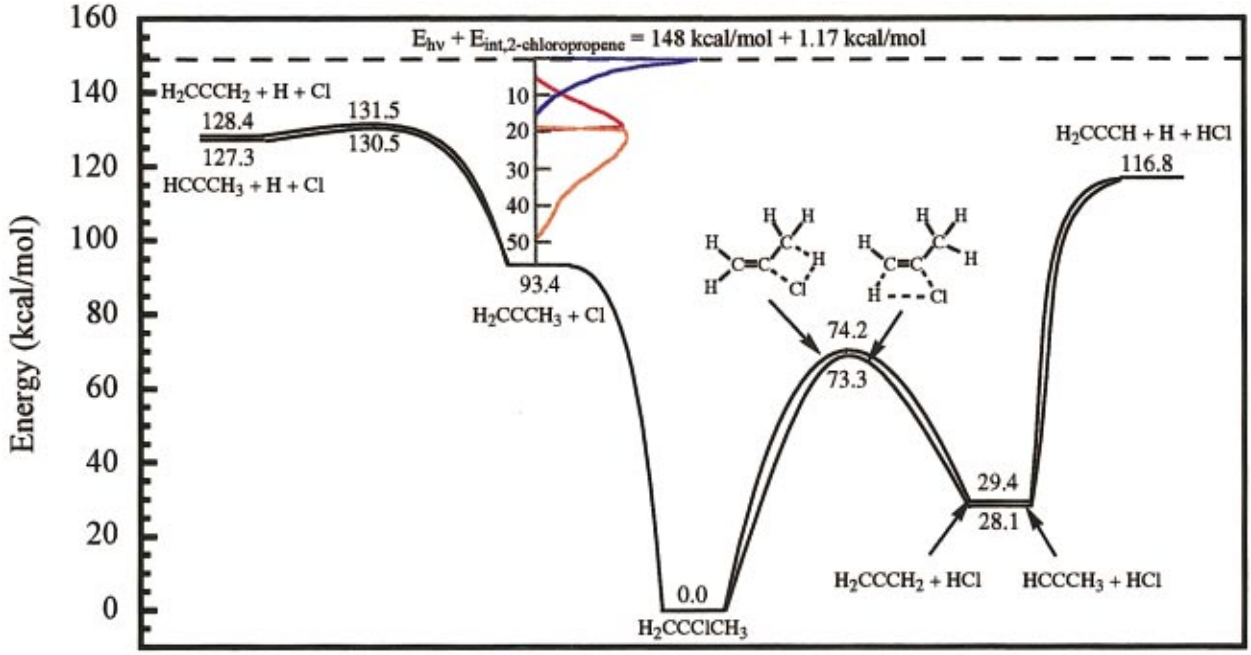

FIG. 1. (Color) Energetics of the 2-chloropropene HCl elimination channels with calculated (Ref. 30) barriers assuming dissociation on the ground-state potential-energy surface, and the C–H fission channels of the 2-propenyl radicals formed from C–Cl fission in 2-chloropropene. The inset shows the product kinetic energies imparted in C–Cl fission (Fig. 5) and producing 2-propenyl radicals in three internal energy groups: a group shown in orange with internal energies below the dissociation limit to H+propyne, a group shown in red with internal energies near but above the dissociation threshold, and the highest internal energy group of radicals (blue), with median internal energy about 15 kcal/mol above the barrier to H+propyne. The barrier energetics shown for the radical dissociation are taken from those calculated in Ref. 1.

changes as a function of internal energy in the radical with an energy resolution of about 3 kcal/mol (even though the radicals are formed with a wide range of internal energies in the primary photolysis step). Comparing the measured change in branching as a function of internal energy to Rice–Ramsperger–Kassel–Marcus (RRKM) predictions allows us to extract information about the relative A-factors of the two decomposition pathways and the relative heights of the barriers to C–H fission from the high-energy 2-propenyl radical isomer. The data thus give an unprecedented window into the unimolecular dissociation reactions of selectively produced hydrocarbon radical isomers.

II. EXPERIMENT

A. UV-vis absorption spectrum and emission spectroscopy

The gas-phase UV-vis absorption spectrum of 2-chloropropene was collected with a HP 8453 Diode-Array UV-Visible Spectrophotometer. 2-chloropropene boils at 295 K, so covering the bottom of a room temperature 1 cm path length cuvette with sample provides enough vapor to acquire the spectrum. The 2-chloropropene in this and all other work described in this paper was purchased from Aldrich (98%) and used without further purification.

The apparatus used to obtain the emission spectrum of 2-chloropropene excited at 199.7 nm has been described previously.[34–36] The laser crosses a free-jet expansion of 41% 2-chloropropene in He through a pulsed valve with 0.5 mm diameter orifice. The gas mix is formed by bubbling He through 2-chloropropene maintained at 0 °C, where its vapor pressure is ~255 Torr; the total pressure of the gas mixture is 615 Torr. We generate the 199.7 nm excitation light by Raman shifting the fourth harmonic of an injection-seeded Nd:YAG laser (Continuum Powerlite 9020) in 50 psi of H_2. An input of about 100 mJ/pulse at 266 nm gives ~100 μJ/pulse at 199.7 nm. The emission from dissociating molecules is imaged into a 0.275 m spectrometer (Acton SpectraPro 275, slit width 3 μm) and dispersed with a 2400 gr/mm holographic grating (Milton Roy) onto an optical multichannel analyzer (EG&G PARC 1456B-990-HQ). With this experimental configuration, our resolution is about 25 cm^{-1} full width at half maximum (FWHM).

B. Photofragment translational spectroscopy

These experiments measure the recoil velocity distributions of fragments from the photodissociation of 2-chloropropene excited at 193.3 nm and the arrival times of the secondary products from the dissociation of 2-propenyl radicals formed in the primary photolysis. We carried out the experiments using the rotating-source, fixed-detector molecular beam apparatus on the Chemical Dynamics Beamline at Lawrence Berkeley National Laboratory's Advanced Light Source (ALS). The key feature of this apparatus, which has been described in detail elsewhere,[32] is that photofragments are ionized in the detector using tunable VUV photons from the ALS rather than by the more traditional electron bombardment method. This ''soft'' ionization largely prevents photofragments from cracking during the ionization

process, making it much easier to identify secondary dissociation products than if electron bombardment ionization is used.

We generate the 11.6% 2-chloropropene–He pulsed molecular beam by bubbling helium through 2-chloropropene cooled to −26 °C and expanding the resulting gas mixture through a General Valve with a 1 mm orifice. With a backing pressure near 800 Torr and a nozzle temperature of about 150 °C there is no evidence of clusters in the molecular beam. Proper analysis of the data requires knowledge of the molecular beam velocity and velocity spread, which we measure by directing the molecular beam straight into the detector and analyzing the shape of the ''hole'' the laser burns into the signal at the parent molecule mass. This procedure gives a peak molecular beam velocity in the number density distribution, $N(v)$, of 1137 m/s and a velocity spread $(\Delta v/v_{\mathrm{pk}})$ of 0.29 with Δv calculated from the full width at half maximum of $N(v)$.

The laser used in this work is a Lambda Physik LPX-200 excimer laser operating on the 193.3 nm ArF transition. Varying the laser power from 1.5 to 36 mJ/pulse showed the dissociation to be the result of single-photon absorption, but saturation effects become significant at the higher powers, so we collect data at laser powers of 5–10 mJ/pulse. The laser beam, focused to a 2 mm×4 mm spot, intersects the molecular beam at an angle of 90°, perpendicular to the plane defined by the molecular beam and the detector axis. Molecules that absorb light dissociate, and a small fraction of the products scatter into the detector, traveling 15.2 cm to the point where they are ionized by tunable VUV radiation from the ALS. The characteristics of the light source have been described in detail elsewhere.[37] The photoionization efficiency curves presented in this paper were taken with a light source bandwidth of 2.2% and most of the photofragment time-of-flight spectra (except the mass 40 10 eV spectrum, as noted in its figure caption) were taken with a light source bandwidth of about 4.5%. A gas filter filled with about 25 Torr Ar eliminates unwanted higher harmonics of the undulator radiation. A MgF_2 window filters out any remaining high-energy photons when the probe energy is below about 10.5 eV.

Ions of the desired mass are selected using a quadrupole mass filter and counted as a function of time using a Daly detector. The previously calibrated ion flight time $(\alpha\sqrt{m_{\mathrm{ion}}})$ constant of $\alpha = 5.81\,\mu\mathrm{s/amu}^{1/2}$ was used to correct for the flight time of the ion through the mass spectrometer; figures show total (ion+neutral) flight times. Rough photofragment angular distribution measurements of the Cl and HCl products showed both to be nearly isotropic, so an anisotropy parameter of 0 is assumed for all product branching determinations.

III. RESULTS AND ANALYSIS

A. UV-vis absorption spectrum of 2-chloropropene

In Fig. 2 we present the UV-vis absorption spectrum of 2-chloropropene from 190 to 300 nm. As expected, it is qualitatively similar to that of vinyl chloride.[38] The main feature to note is the first strong absorption band growing in near 220 nm. We believe the structure at the top of the peak may be the vibrational structure of the predissociative electronic state accessed in the absorption. The spectrum between 300 and 1100 nm, also acquired but not shown in the figure, displays no absorption features detectable with our spectrometer.

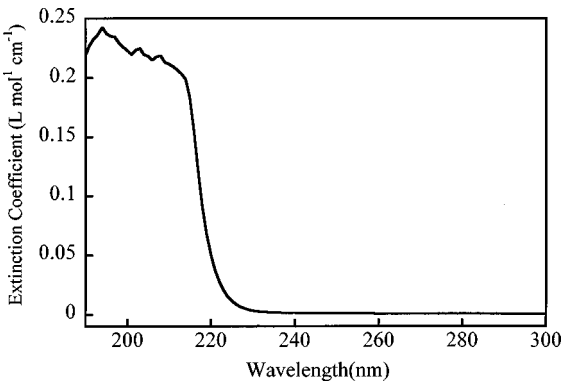

FIG. 2. Absorption spectrum of gaseous 2-chloropropene. The spectrometer is likely saturated just below 220 nm, as we expect the $\pi\pi^*$ absorption to be as strong as in vinyl chloride.

B. Emission spectroscopy of 2-chloropropene excited at 199.7 nm

Figure 3 shows the emission spectrum of dissociating 2-chloropropene excited at 199.7 nm. The spectrum is similar to the emission spectrum of vinyl chloride.[35] We assign the strongest feature, appearing near 1625 cm^{-1}, to ν_5 (the C═C stretch) with a literature value of 1640 cm^{-1}.[7] The peaks at 3256 and 4880 cm^{-1} thus correspond to $2\nu_5$ and $3\nu_5$, respectively. Two quanta of ν_{19}, the C═C twist, (literature value of $\nu_{19} \approx 692\,\mathrm{cm}^{-1}$, $2\nu_{19} \approx 1384\,\mathrm{cm}^{-1}$)[7] give rise to the peak at 1378 cm^{-1}. The feature near 2990 cm^{-1} is assigned as ν_3, the CH_2 symmetric stretch, which has a literature value of 2992 cm^{-1}.[7] Finally, we assign the peak at 646 cm^{-1} as ν_{12}, the C–Cl stretch (literature value of 641 cm^{-1}).[7] To understand the observed absorption and emission spectra, we performed configuration interaction with single

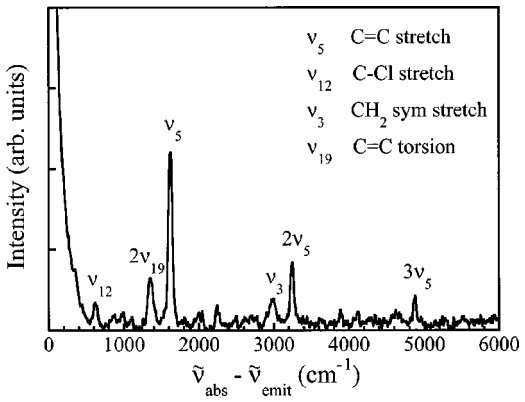

FIG. 3. Emission spectrum of gaseous 2-chloropropene excited at 199.7 nm, plotted as a function of the wave number of the absorbed photon minus the wave number of the emitted photon (the Raman shift).

electron excitations (CIS) *ab initio* calculations using GAUSSIAN 98[39] to characterize the nature of the electronic transition near 200 nm. We used the MP2/6-311G(d,p) [(MP2) second-order Moller–Plesset] optimized geometry from GAMESS-US[40] for these calculations.[30] The CIS calculation, restricted to singlet spin states, gave a vertical excitation energy to the bright state of 7.8411 eV, thus overestimating it by the 1 to 2 eV typical for CIS calculations, and identified the electronic character of the transition as primarily $\pi\pi^*$, similar to that in vinyl chloride. Thus, the forces in the Franck–Condon region act to stretch the C=C bond, resulting in the strong emission to the ν_5 feature as also observed in vinyl chloride.[35]

C. Photofragment translational spectroscopy of 2-chloropropene

The data show evidence for several primary reaction channels: C–Cl fission (3), HCl elimination [(6) and (8)], and a minor C–CH_3 fission channel (1), as well as several subsequent secondary dissociation processes, as detailed below. Contributions from Reactions (10)–(13), which involve loss of H and H_2, may only be detected in the data presented here if the dissociation releases considerable energy to product translation. Time-of-flight (TOF) spectra collected for 30 000 laser shots at $m/e=75(C_3H_4Cl^+)$ and $74(C_3H_3Cl^+)$ and a source angle of 5° show no significant signal, so if any products from loss of H or H_2 are formed, those dissociations must not be releasing more than 6.69 and 3.3 kcal/mol, respectively, to product translation.

1. Atomic chlorine loss and subsequent secondary dissociation of the 2-propenyl radical

In Fig. 4 we show the TOF spectra of $m/e=35(Cl^+)$ collected for 200 000 shots at source-detector angles of 15° and 35° and a photoionization energy of 13.5 eV. Two main peaks are evident: A sharp, fast one centered at ~100 μs and a broad, slow one near 150 μs. Figure 5 shows the $P(E_T)$'s obtained by forward convolution fitting of the $m/e=35$ spectra. Note that the two fast $P(E_T)$'s shown in orange and red combine to give a single peak. We treat the two components separately rather than combining them into one distribution because the C–Cl fission reactions releasing the largest energies to product translation (the Cl atoms from which are shown in the orange line) give momentum-matched mass 41 partner radicals with internal energies low enough that they are stable to secondary dissociation. The TOF spectra of $m/e=41$, $C_3H_5^+$ at angles of 15° and 35° and photoionization energies of 10.5 eV (with the MgF_2 window) shown in Fig. 6 thus contain only a single, sharp peak which is fit by the orange $P(E_T)$ in Fig. 5. This $P(E_T)$ corresponds to C–Cl fission that releases enough energy to product translation to produce a stable 2-propenyl radical. The fits to the mass 35 spectrum show that about 50% of the C–Cl bond fission events yield stable 2-propenyl products. (If the 2-propenyl radicals formed in the chlorine loss channel were all stable to secondary dissociation, no peaks should appear in the Cl^+ spectra that do not also appear in the 2-propenyl spectra except a small contribution from secondary dissociation of C_2H_2Cl, R2). 2-propenyl radicals momentum-matched to the slowest Cl atoms (27% of C–Cl fission events, shown in blue) and the slower of the two groups of Cl atoms contributing to the fast peak in Fig. 4 (23% of C–Cl fission events, shown in red) are formed with enough internal energy to dissociate, and do so. As a result, they are not detected at mass 41, but rather at the secondary product masses. Three secondary dissociation channels are energetically allowed and potentially viable from a C_3H_5 isomer: H atom loss to make allene, H atom loss to make propyne, and C–C bond fission to $CH_3+C_2H_2$. (The barriers to H_2 elimination are likely to be considerably higher.) Figure 7 shows the $m/e=40(C_3H_4^+)$ TOF spectra obtained at a photoionization energy of 11 eV. Two main peaks appear in these spectra: A sharp, fast one near 100 μs and a broad, slow one centered at 150 μs. The two slower $P(E_T)$ distributions shown in red and blue in Fig. 5 fit these peaks. This is to be expected, as the recoil velocity imparted to the mass 40 product from the

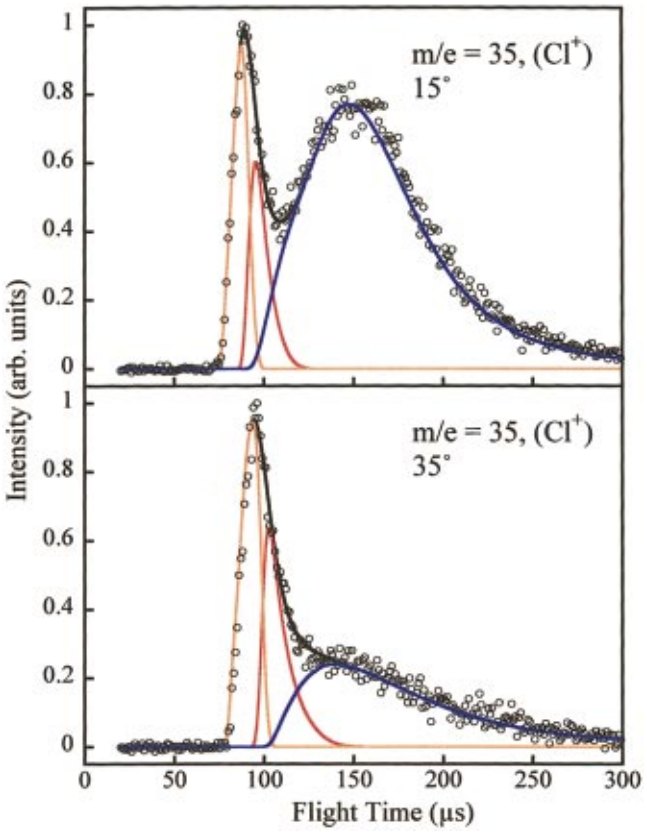

FIG. 4. (Color) Time-of-flight spectra collected with a photoionization energy of 13.5 eV of the $m/e=35$ signal with source angle shown. The signal is assigned to VUV ionization of the ^{35}Cl atom photofragments from C–Cl bond fission in 2-chloropropene. Experimental data is shown with open circles. Fits shown are calculated from the C–Cl bond fission product translational energy distributions shown in Fig. 5 (and in the inset in Fig. 1). Since lower internal energy momentum-matched 2-propenyl radicals are produced when more energy is imparted to translation in the C–Cl fission, the orange fit shows the Cl atoms momentum-matched to the stable mass 41 2-propenyl radicals (see Fig. 6), the red fit shows the Cl atoms momentum-matched to near-threshold but dissociative 2-propenyl radicals that undergo C–H bond fission and give mass 40 allene/propyne products (see red contribution in Fig. 7), and the blue fit shows the Cl atoms momentum-matched to higher internal energy dissociative 2-propenyl radicals that also undergo C–H bond fission and give mass 40 allene/propyne products (see blue contribution in Fig. 7). Figure for 15° angle is adapted from Ref. 33 with permission of the authors.

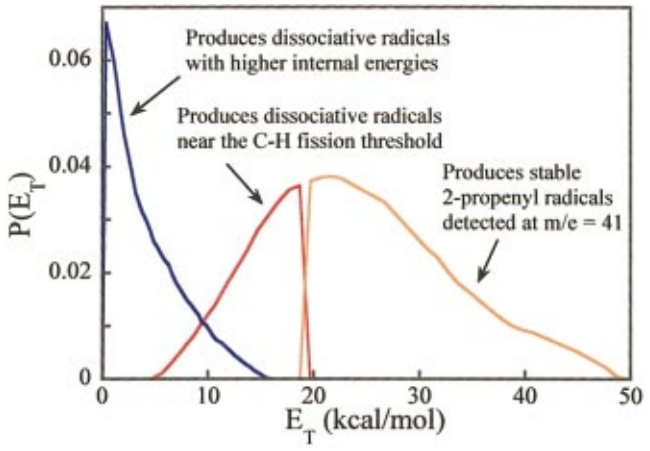

FIG. 5. (Color) Product kinetic energy distributions, $P(E_T)$, for C–Cl bond fission in the 193 nm photodissociation of 2-chloropropene derived from forward convolution fitting of the signal in Fig. 4. These C–Cl bond fission distributions produce three groups of momentum matched 2-propenyl radical products in a ratio of 49.7% (orange): 23.0% (red): 27.3% (blue). The orange $P(E_T)$ derived from fitting the fastest signal in the Cl atom TOF fits the remaining stable mass 41 products. The red and the blue $P(E_T)$'s produce dissociative 2-propenyl radicals with, respectively, near threshold internal energies and internal energies centered on an energy 15 kcal/mole higher than the barrier to C–H fission in the radical, so the momentum-matched partner dissociates and does not contribute to the mass 41 spectrum in Fig. 6. However, since C–H bond fission in the dissociative radicals does not alter the mass 40 product's velocity from the velocity the parent radical had from the precursor's C–Cl bond fission, we can predict the arrival times in Fig. 7 of the mass 40 products from the radical dissociation from the red and blue $P(E_T)$'s and in this way identify the internal energy of the radical that resulted in propyne or allene product at each arrival time in the mass 40 TOF spectrum in Fig. 7.

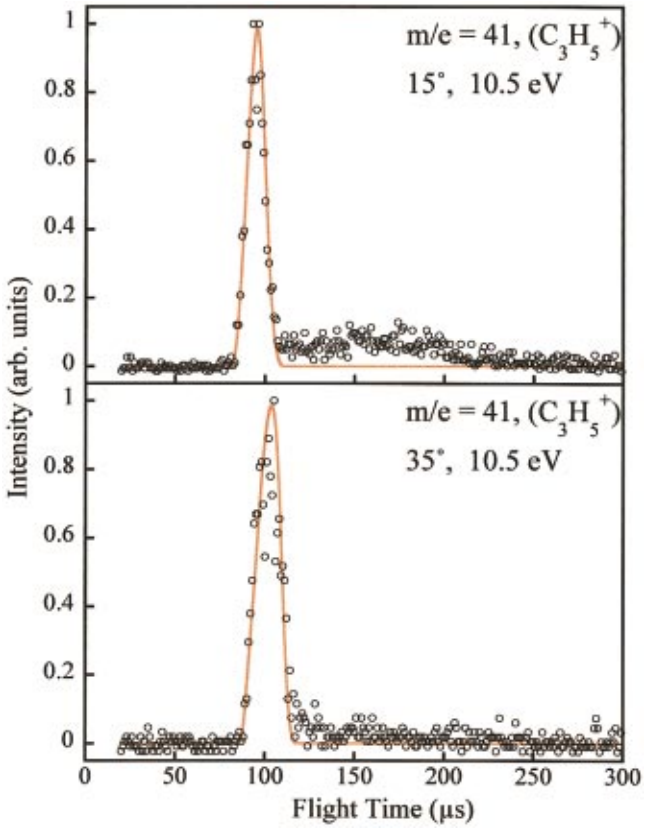

FIG. 6. (Color) Time-of-flight spectra collected with a photoionization energy of 10.5 eV of the $m/e=41$ signal with source angles shown. The signal is assigned to VUV ionization of the stable C_3H_5 radicals from C–Cl bond fission events in 2-chloropropene releasing more than about 19 kcal/mol of energy to product translation. Experimental data is shown with open circles. Fit shown is calculated from the orange C–Cl bond fission product translational energy distribution shown in Fig. 5.

C–H fission in 2-propenyl radical dissociation is so small (mass 1 recoiling from mass 40) that the mass 40 propyne/allene product must travel at essentially the same velocity as its particular parent 2-propenyl radical. Thus, the time-of-arrival of each mass 40 product gives essentially no information on the energy partitioned to product translation in the secondary dissociation, but it gives us critical information on the internal energy of the parent 2-propenyl radical from which the mass 40 product came. The arrival time distribution of the propyne versus allene products from the 2-propenyl radicals dispersed by internal energy in the primary C–Cl photolysis step thus gives us a direct measure of the change in branching between the H+propyne and the H+allene radical dissociation channels as a function of the internal energy in the radical. We exploit this, as discussed below. Note that very few, if any, 2-propenyl radicals undergo C–C bond fission, since retaining the same relative probabilities of the slowest (27%) and near-threshold (23%) 2-propenyl radical products (as predicted from the relative intensities of the Cl atom momentum matched partners) gives the good fit shown in Fig. 7 to the mass 40 secondary products from each group of radicals. The shoulder on the fast side of the 100 μs peak in Fig. 7 results from propyne/allene produced in primary HCl elimination. This will be discussed further in Sec. III B 2.

We tried two different approaches to determining how the branching between the H+allene and the H+propyne channel from the dissociation of the 2-propenyl radical changes with internal energy in the radical. First, we obtain photoionization efficiency (PIE) curves by measuring, as a function of photoionization energy, the amount of $m/e=40$ signal arriving in a particular time gate. Proper choice of the time gate allows us to examine the allene/propyne dissociation products from the near-threshold internal energy 2-propenyl radicals separately from the allene/propyne products from higher internal energy 2-propenyl radicals. (The products with arrival times between 120 and 300 μs are from the higher internal energy group of 2-propenyl radicals, with median internal energy 15 kcal/mol above the C–H fission barrier.) Figure 8 shows the photoionization efficiency curves obtained for various time gates of the $m/e=40$ signal. For comparison, Fig. 9 shows the photoionization efficiency curves of molecular beams of pure allene (I.E.$=9.69$ eV)[41] and pure propyne (I.E.$=10.36$ eV)[41] with the same bandwidth photoionization source. Certainly, the partial PIE curves of the mass 40 signal from the dissociation of both the near-threshold 2-propenyl radicals and the higher internal energy radicals are due primarily to propyne, but some allene is likely formed as well. At first glance, one might expect that taking the right linear combinations of the pure allene and propyne curves should generate composites looking like the $m/e=40$ curves. Unfortunately, no combinations of the pure cold allene and cold propyne photoionization curves yielded

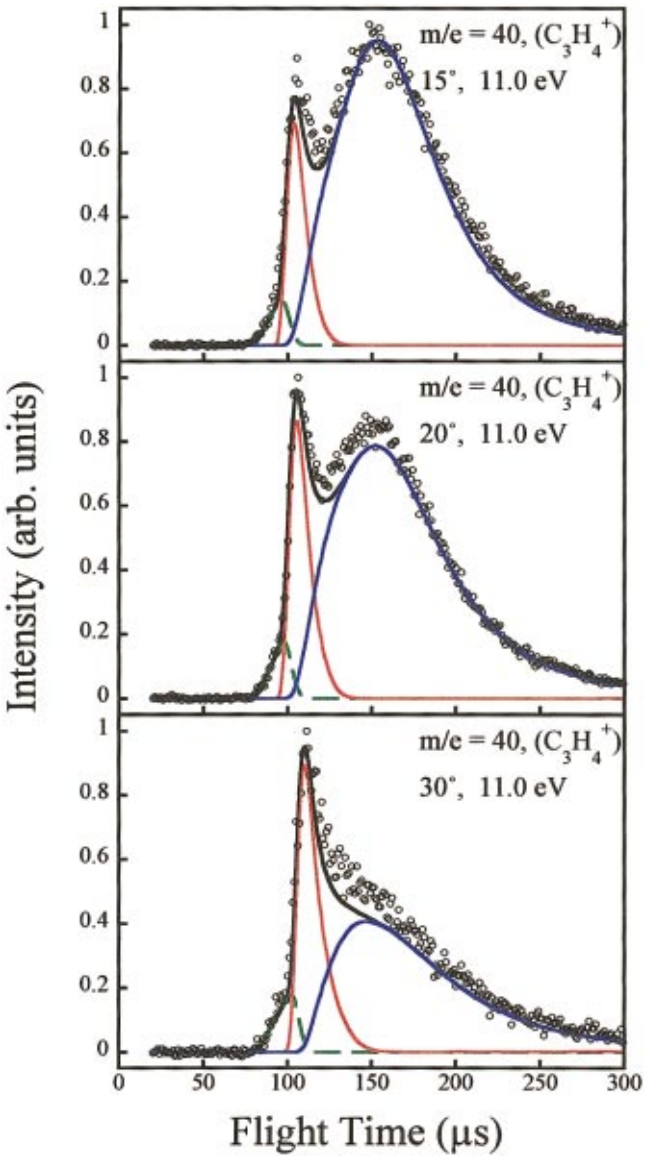

FIG. 7. (Color) Time-of-flight spectra collected with a photoionization energy of 11.0 eV of the $m/e=40$ signal with source angles shown. The signal is assigned to VUV ionization of the allene/propyne products from the unimolecular dissociation of 2-propenyl radical formed from C–Cl bond fission in the 2-chloropropene precursor and from primary HCl elimination from 2-chloropropene. Experimental data is shown with open circles. The red and the blue fits shown predict the arrival times of the allene/propyne secondary product from the 2-propenyl radical dissociation by noting that the velocity of the allene/propyne secondary product should be nearly identical to that of the 2-propenyl radical from which it came. Thus the fit shown in red line for the products from near-threshold radical dissociation and the fit in blue line for products from the dissociation of higher internal energy 2-propenyl radicals is derived from the corresponding color C–Cl bond fission $P(E_T)$ for the two groups of dissociative radicals shown in Fig. 5. The fits use a predetermined relative amount of the mass 40 propyne/allene product from the higher internal energy radicals (blue line) to near threshold allene/propyne products (red line) of 1.185 as obtained, with correction for kinematic factors in the three-dimensional (3D) scattering, from the ratio of the Cl atoms momentum-matched to the two groups of dissociative radicals. The appropriateness of using this fixed ratio relies on the assumption that the radicals dissociate only via C–H fission (negligible C–C fission) and that the detection efficiency for allene at 11 eV photoionization energy is similar to that of propyne. The fit shown in long-dashed green line for the mass 40 products from HCl elimination that survive secondary dissociation is calculated from the long-dashed green line portion of the $P(E_T)$ in Fig. 13. Figure for 20° angle is adapted from Ref. 33 with permission of the authors.

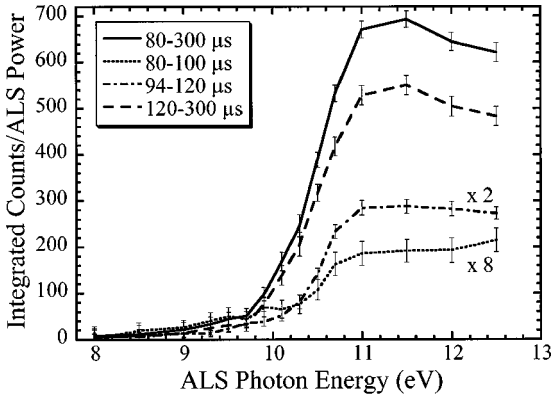

FIG. 8. Photoionization efficiency curves for mass 40 products detected at a source angle of 20° and integrated over flight times shown in the legend. (For corresponding flight time ranges, see 20° mass 40 spectrum shown in the middle frame in Fig. 7.) Data was taken with the narrower energy linewidth and corrected for VUV energy. Data points shown with error bars and with straight-line extrapolations between each point to guide the eye. In the data shown, points below 10.5 eV were taken with the MgF_2 filter in the photon beam (see the Experiment section); points at 10.5 eV and above were taken without the filter. The figure is reproduced from Ref. 33 with permission of the authors.

results that looked even remotely like the experimental curves, probably because the allene and propyne photofragments are formed with significant vibrational excitation. This causes their ionization onsets, particularly that of allene, to be red-shifted from those of the pure compounds, so the photoionization efficiency curve of vibrationally excited allene products is expected to have a more gradual onset and be significantly red-shifted from that of colder allene shown in Fig. 9. Thus, instead of simulating the photoionization curves to determine the fraction of allene in the mass 40 products from the lower and higher-internal-energy radicals, we sought to extract how the branching ratio changes as a function of internal energy in the radical. To do this, we retook the 20° data at $m/e=40$, but tuned the photoionization energy to 10 eV in order to detect allene, but not

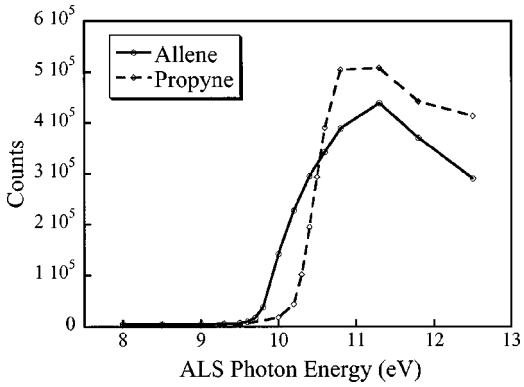

FIG. 9. Photoionization efficiency curves of pulsed beams of allene and propyne. Data was taken with the narrower ALS linewidth used also in Fig. 8 and corrected for VUV energy. Points below 10.6 eV were taken with the MgF_2 filter in the ALS beam (see the Experiment section); the points at 10.6 eV are averages of the counts measured with and without the MgF_2 filter; and the points above 10.6 eV were taken without the MgF_2 filter. The neat allene and propyne beams were formed under modest expansion conditions (stagnation pressure=340 Torr and nozzle at room temperature), so vibrational cooling of these molecules is not dramatic.

propyne, products from 2-propenyl radical dissociation. This spectrum is shown in Fig. 10. It is clear by inspection that the quantum yield of allene from the group of radicals with higher internal energy is higher than the quantum yield of allene from the group of radicals with lower internal energy. Using the two kinematically corrected probability ratios obtained from fitting the relative intensities of the fast and slow peaks in each spectrum (Figs. 7 and 10)

$$\frac{\left(\frac{\phi_{\text{allene}}}{\phi_{\text{allene}}+\phi_{\text{propyne}}}\right)_{\text{high } E_{\text{int}} \text{ radicals}}}{\left(\frac{\phi_{\text{allene}}}{\phi_{\text{allene}}+\phi_{\text{propyne}}}\right)_{\text{low } E_{\text{int}} \text{ radicals}}} = \frac{\left(\frac{(\phi_{\text{allene}})_{\text{high } E_{\text{int}} \text{ radicals}}}{(\phi_{\text{allene}})_{\text{low } E_{\text{int}} \text{radicals}}}\right)}{\left(\frac{(\phi_{\text{allene}}+\phi_{\text{propyne}})_{\text{high } E_{\text{int}} \text{ radicals}}}{(\phi_{\text{allene}}+\phi_{\text{propyne}})_{\text{low } E_{\text{int}} \text{ radicals}}}\right)} = \frac{(2.39)}{(1.185)} = 2.0(+0.05/-0.15),$$

gives the following change in branching to the H+allene channel with internal energy of the dissociating radical:

Thus, we experimentally determine that the fraction of 2-propenyl radicals that dissociate to give H+allene products is 2.0 (+0.05/−0.15) times larger for dissociation of the group of radicals with higher internal energy (median energy 15 kcal/mole above the barrier to H+propyne) than from the group of radicals with lower internal energy. This experimental result is in reasonable agreement with the RRKM prediction of 2.2 for the change in yield of H+allene products as the internal energy of the dissociating group of radicals is changed from the near-threshold distribution to the higher-energy distribution having median internal energy 15 kcal/mol above the barrier. We give further information on the RRKM calculations below. Although we cannot obtain an absolute branching ratio between the 2-propenyl secondary dissociations forming allene, (4), and propyne, (5), we can use RRKM theory to predict the rates for formation of allene and propyne in the products from the near-threshold internal energy radicals. We can then derive, from how the relative intensities of the peaks in Fig. 7 change in going to the 10 eV spectrum in Fig. 10, what the experimental branching to the H+allene channel is for the higher internal energy group of radicals. Assuming ϕ_{allene} is 10.3 (±2)% from the near-threshold internal energy group of radicals, as determined from the RRKM calculations, the relative intensities of the signal in the mass 40 spectrum at 10 eV photoionization energy show the branching to the H+allene channel increases to [10.3(±2)%(2.015)=21(±4)%] for dissociation of the higher internal energy group of 2-propenyl radicals. This result is consistent with the partial PIE curve of the products from the group of radicals with higher internal energy and arrival times between 120 and 300 μs, which has an ionization onset at slightly lower energies than the faster, near-threshold group.

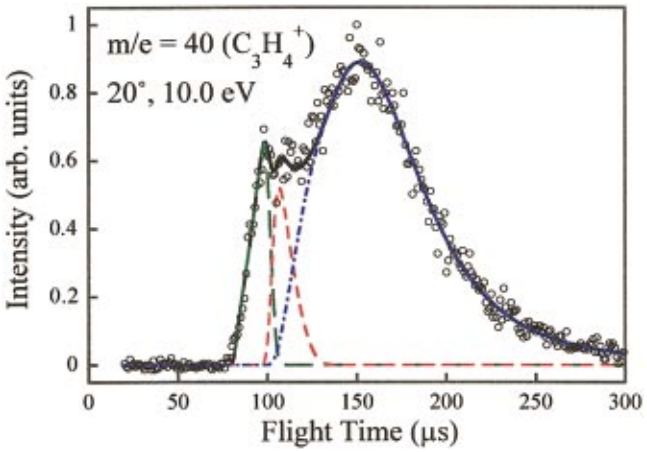

FIG. 10. (Color) Time-of-flight spectrum of the allene products from the unimolecular dissociation of 2-propenyl radicals formed from C–Cl bond fission in the 2-chloropropene precursor and from the allene/propyne products from primary HCl elimination from 2-chloropropene that are stable to secondary dissociation. The spectrum was collected by integrating the signal for 3×10^6 laser shots at a source angle of 20° with a photoionization energy of 10.0 eV and with small light source apertures (4 mm×5 mm) to achieve a narrow (2.2%) bandwidth. Experimental data is shown with open circles. The red-dashed fit for the arrival times of the allene secondary product from the dissociation of near-threshold 2-propenyl radicals is calculated from the partial C–Cl primary bond fission $P(E_T)$ in red-dashed line in Fig. 11 corresponding to C–Cl bond fission events that produced dissociative 2-propenyl radicals near threshold that went on to dissociate to H+allene. The blue–dot–dashed fit for the arrival times of the allene secondary product from the dissociation of higher internal energy 2-propenyl radicals is calculated from the partial C–Cl bond fission $P(E_T)$ in blue-dot–dashed line in Fig. 11 corresponding to primary C–Cl bond fission events in 2-chloropropene that produced higher internal energy dissociative 2-propenyl radicals that went on to dissociate to H+allene. The green dashed-line fit shown for the allene/propyne products from HCl elimination that survive secondary dissociation is calculated from the higher energy portion of the HCl elimination $P(E_T)$ in Fig. 13 shown in green dashed-line. Figure is adapted from Ref. 33 with permission of the authors.

More information on the internal energy dependence of the branching between the H+allene and H+propyne channels from the dissociation of 2-propenyl radicals is apparent in fitting the velocity distribution of the allene products from the near-threshold internal energy dissociative 2-propenyl radicals. While fits of the mass 41 and mass 35 signal showed that 2-propenyl radicals could be formed with enough internal energy to dissociate from primary C–Cl bond fission events releasing less than 18.4 kcal/mol (or a bit higher) in translation, acceptable fits of the allene data in Fig. 10 could not be achieved until we assumed the internal energy required to access the H+allene channel was higher. The short-dashed line $P(E_T)$ in Fig. 11 that fit the arrival times of the allene products from low internal energy dissociative C_3H_5 shows this clearly; H+propyne products appeared as products from radicals with higher kinetic energies near 19 kcal/mol, corresponding to a lower internal energy, than did H+allene products. Thus, the barrier to H+allene formation is higher than the barrier to H+propyne formation.

In addition, we could not fit the data in Fig. 10 acceptably by assuming the branching to the H+allene channel was constant for the products from the low internal energy group of radicals shown in red (although this gave a decent fit for the higher internal energy group of radicals shown in blue,

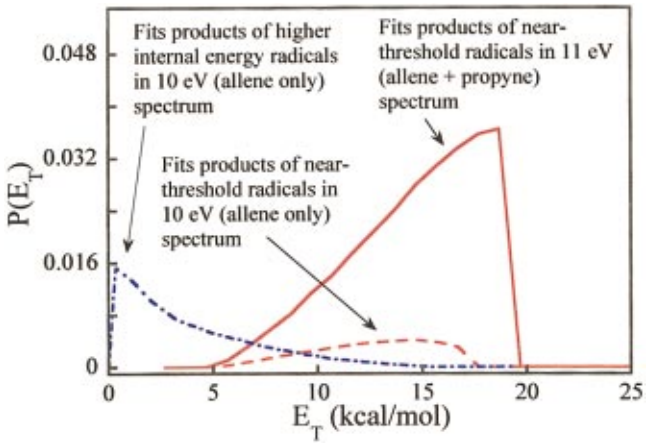

FIG. 11. (Color) Partial product kinetic energy distributions for the C–Cl bond fission events that produced 2-propenyl radical that went on to dissociate to H+allene are shown in red dashed and blue dot-dashed line. These $P(E_T)$'s gave a good fit to the arrival times of the secondary allene products in the mass 40 time-of-flight spectrum taken at 10 eV photoionization energy shown in Fig. 10. Comparison of the red-dashed C–Cl fission $P(E_T)$ that fit the allene signal in Fig. 10 with the solid line red $P(E_T)$ taken from Fig. 5 that fit the total propyne+allene signal from the dissociation of near-threshold dissociative radicals from C–Cl fission shows that the barrier to H+allene is higher than the barrier to H+propyne and that the branching to H+allene increases with increasing internal energy in the dissociative radical. Iteratively tested by forward convolution fitting the data in Fig. 10, the shape of both partial $P(E_T)$'s shown were calculated by weighting the number of dissociative radicals at each internal energy (shown in Fig. 5 and derived from the Cl atom TOF) with the fractional RRKM rate constant for allene formation, but only the fit of the time-of-arrival of the near-threshold allene products was sensitive to this weighting. Accounting for kinematic factors in the 3D scattering, the relative yield of allene product from the higher internal energy radicals to near threshold allene products was determined to be 2.39 by varying the ratio to obtain the best fit to the spectrum in Fig. 10. Figure is adapted in part from Ref. 33 with permission of the authors.

where the change in branching as a function of internal energy is expected to be slower). A much better fit to the data was obtained when we assumed the branching to the H+allene channel increased with increasing internal energy of the radical even within the group of allene/propyne products from the low internal energy group of 2-propenyl radicals. In other words, when fitting the allene products resulting from the radicals with near-threshold internal energy, we did not use a constant 10.3% fraction of the $P(E_T)$ (shown in red in Fig. 5) that fit the total allene+propyne spectrum shown in Fig. 7. Instead, the $P(E_T)$ that fits the allene products of the near-threshold group of 2-propenyl radicals was obtained by weighting the red distribution in Fig. 5 with calculated RRKM rate constants to determine, at each internal energy, the fraction that gives allene products. The weighting factor is just $k_{\text{allene}}/(k_{\text{allene}}+k_{\text{propyne}})$. Ignoring the parent 2-chloropropene molecules' spread in internal energy, we crudely identified the 2-propenyl radicals formed from primary C–Cl bond fission releasing 17.4 kcal/mol in translation as having an internal energy 0 kcal/mol above the barrier to H+allene and 1 kcal/mol above the barrier to H+propyne. These barriers were used to obtain the pairs of energy-specific RRKM rate constants needed to calculate the weighted $P(E_T)$ in Fig. 11 (dashed red line) that fit the allene products' arrival times in Fig. 10. (In reality, we observe some propyne products from 2-propenyl radicals from primary photolysis events that released more than 18.4 kcal/mol to translation because some of the 2-propenyl radicals come from 2-chloropropene precursors with internal energy higher than the most-probable value.)

In summary, we obtain good fits to the arrival times of allene derived from near-threshold 2-propenyl radicals only if we assume: (i) The barrier to H+allene is higher than the barrier to H+propyne and (ii) the branching to the H+allene channel increases with internal energy above the H+allene barrier. In the discussion we compare the barriers obtained in fitting the data in this way with those predicted from a combination of thermodynamics and density-functional theory calculations.

2. HCl elimination and subsequent secondary decomposition of the m=40 product

The $m/e=36(HCl^+)$TOF spectra acquired at source angles of 20° and 40° (photoionization energy=13.5 eV, 200 000 shots) exhibit single, broad peaks centered near 110 μs, as shown in Fig. 12; the $P(E_T)$ used to fit these spectra appears as the solid green line in Fig. 13. The photoionization efficiency curve of the HCl product is shown as the dashed line in Fig. 14. Taking into account the energy width of the ALS, the HCl reaction product shows a photoionization onset of 10.5 eV, over 2.2 eV lower than the usual ionization potential of 12.74 eV.[41] Given the large H–Cl separation in the transition state, one would expect the HCl formed in the elimination process to be vibrationally excited. The redshift of the ionization onset, also apparent in the HCl product from vinyl chloride photolysis,[23] indicates that the HCl product is indeed internally excited; unfortunately, there is currently no method for obtaining the degree of vibrational excitation of a molecule from its photoionization spectrum.

To identify the mass 40 momentum-matched partner to the HCl from primary HCl elimination, we can use the $P(E_T)$ in Fig. 13 to predict its time-of-flight spectrum. However, note that if propyne/allene is formed with about 89 kcal/mol of internal energy it will dissociate to propargyl+H,[15] and that the energy partitioned to internal energy of the HCl elimination products is roughly 124 kcal/mol-E_T (using the parent precursor's most probable internal energy of 1.2 kcal/mol). Thus we expect the later-arriving allene/propyne products to be lost to secondary dissociation to propargyl radical (mass 39)+H if the HCl partner does not carry away more than 35 kcal/mol of internal energy. We can characterize the mass 40 products lost in this way by measuring the spectrum at mass 39. Thus, the fast shoulder to the sharp peak centered at 100 μs in Fig. 7, the $m/e=40$ spectrum, momentum-matches to the HCl, as these allene/propyne products are formed with internal energies low enough that they are stable to secondary dissociation. However, as expected, in order to obtain a satisfactory fit to the $m/e=40$ data, we need to truncate the $P(E_T)$ used to fit the $m/e=36$ data. This truncated $P(E_T)$, shown in dashed green line in Fig. 13, represents about 40% of the allene/propyne products. About 60% of the allene and propyne formed in the HCl elimination reaction thus had sufficient energy to undergo secondary loss of a hydrogen atom to

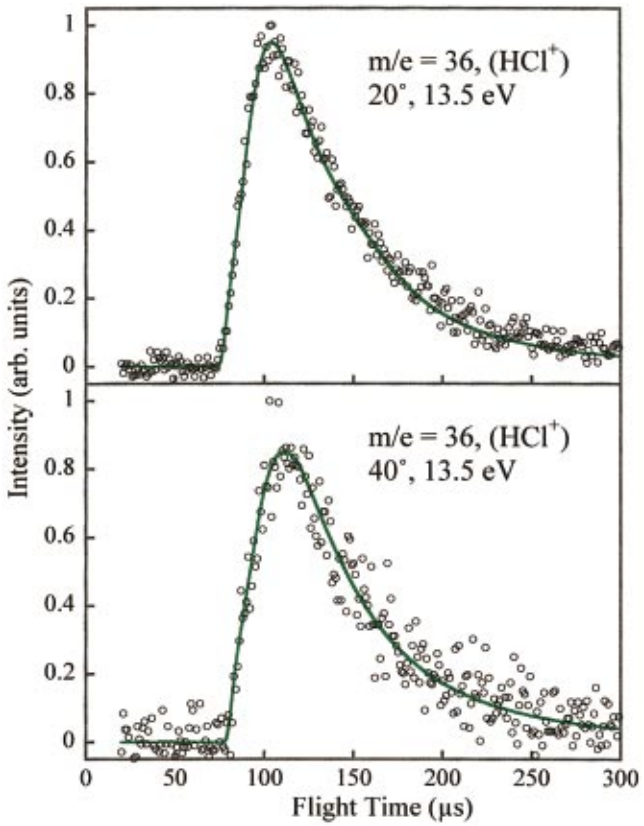

FIG. 12. (Color) Time-of-flight spectra of the HCl products from primary HCl elimination from 2-chloropropene. The spectrum was collected with a photoionization energy of 13.5 eV at the source angles shown. Experimental data is shown with open circles. The green line fit for the arrival times of the HCl product is calculated from the total HCl elimination $P(E_T)$ in solid green line in Fig. 13.

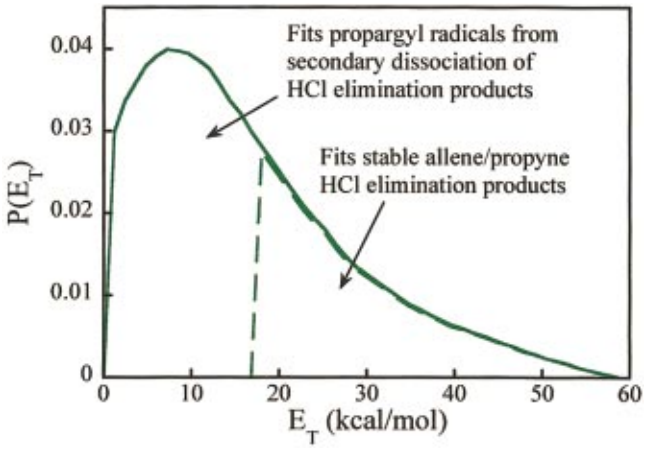

FIG. 13. (Color) Product kinetic-energy distribution, $P(E_T)$, for primary HCl elimination from 2-chloropropene in green solid line derived from forward convolution fitting of the signal in Fig. 12. Some of the momentum-matched allene/propyne undergoes secondary dissociation to propargyl+H so the flight time of the remaining stable allene/propyne in Figs. 7 and 10 are fit with the higher energy part of this shown in green-dashed line. The remaining lower energy part of the $P(E_T)$ adequately predicts the arrival times of the propargyl secondary product as shown in green dot–dashed-line in Fig. 15 (since losing an H from allene/propyne results in propargyl radicals traveling with essentially the same velocity as the propargyl from which it came), but the mass 40 products and the mass 39 secondary products may also be fit with partial $P(E_T)$'s that overlap more significantly.

yield propargyl radicals, detected at $m/e=39$, $C_3H_3^+$, the spectrum of which is shown in Fig. 15. Fortunately, this secondary dissociation gives mass 39 products with essentially the same time-of flight distribution as the mass 40 HCl elimination products would have had (as with the 2-propenyl radical's secondary dissociation, loss of an H atom barely changes the heavier product's velocity). Therefore, one can identify the signal from propargyl radicals formed in this secondary dissociation by using the portion of the HCl elimination $P(E_T)$ not used in fitting the stable mass 40 HCl elimination products in the $m/e=40$ TOF spectrum; the predicted time-of-flight distribution of the secondary propargyl radicals is shown in the green dot-dashed line in Fig. 15. Although the truncation point in the HCl elimination $P(E_T)$ is shown as rather sharp in Fig. 13, a more gradual transition between stable and unstable mass 40 HCl elimination products can also fit the data, as one would expect if the HCl product is formed with a distribution of internal energies. Using the very uncertain sharp truncation near 17 kcal/mol in translation suggests the HCl co-fragment carriers away typically about 18 kcal/mol of internal energy. The very large redshift in the ionization onset observed in the photoionization spectrum of the HCl product implies, however, that some HCl product is probably formed with much higher internal energy. The remaining signal in the $m/e=39$ TOF spectrum in Fig. 15 is adequately fit by assuming it results from a daughter ion of the stable mass 41 neutral 2-propenyl radicals also detected at parent mass in Fig. 6. Although there are no prior experimental results on the ionization energy of the 2-propenyl radical or the appearance energies of its ion daughters, observing a $C_3H_3^+$ daughter ion from highly vibrationally excited (within 0–20 kcal/mole of the H+propyne barrier) 2-propenyl radicals is not too surprising. The cyclic $C_3H_3^+$ ion is resonance stabilized and the spectrum in Fig. 15 is taken at a photoionization energy of 11 eV, considerably higher than the expected ionization energy of the 2-propenyl radical of about 8 eV,[42] so is likely above the appearance energy of the stable[43] cyclic $C_3H_3^+$ daughter ion. A preliminary photoionization efficiency

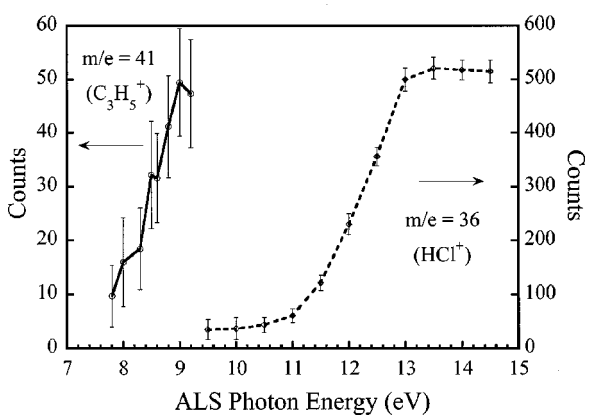

FIG. 14. Photoionization efficiency curves for mass 41 products and mass 36 products detected at a source angle of 20°. Data was taken with the narrower energy linewidth and corrected for VUV power. Data points shown with error bars and with straight-line extrapolations between each point to guide the eye. The MgF_2 filter (see Experiment) was used when acquiring the $m/e=41$ data, but not for the $m/e=36$ data.

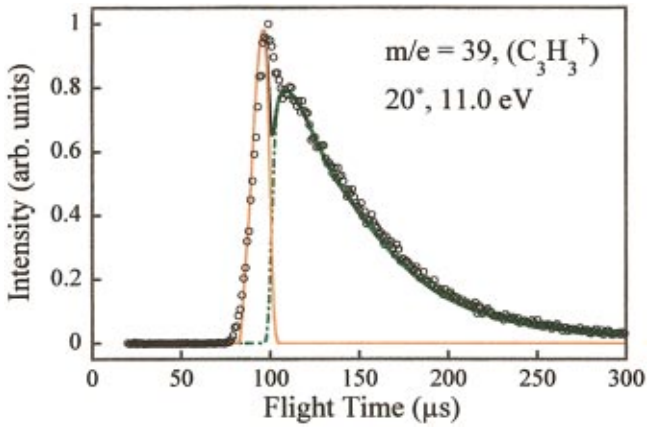

FIG. 15. (Color) Time-of-flight spectrum of photofragments giving signal at $m/e=39$, $C_3H_3^+$ showing a contribution in green from the C_3H_3 neutral propargyl products from the secondary dissociation of propyne/allene from HCl elimination events releasing smaller amounts of energy to kinetic energy (see Fig. 13, caption), and a contribution in orange from the dissociative ionization of the stable 2-propenyl radical, from primary C–Cl fission. Experimental data are shown with open circles. The figure is adapted from Ref. 33 with permission of the authors.

curve of the stable, but highly vibrationally excited, 2-propenyl radicals is shown as the solid line in Fig. 14; it is likely redshifted from what the spectrum of the cold radicals would be.

In determining whether the primary HCl elimination from 2-chloropropene excited at 193 nm produces allene+HCl(6) or propyne+HCl(8), two factors must be considered. First, not only are about 60% of the elimination products formed with sufficient internal energy (89 kcal/mol)[16] to undergo secondary dissociation to propargyl+H, but also the isomerization barrier between allene and propyne is around 65 kcal/mol.[1,27–29] Thus, we can only measure the branching between the two HCl elimination channels for the events that produce propyne/allene products stable to secondary dissociation, and a significant fraction of these may isomerize before we detect them. We expect the equilibrium between the two C_3H_4 isomers to favor propyne, both because propyne is lower in energy by about 1 kcal/mole, and more importantly, because propyne has an internal rotor that increases its statistical weight in the loose transition state. In addition, the propyne/allene product not lost to secondary dissociation typically still has much higher internal energy than the propyne and allene from secondary dissociation of the 2-propenyl radicals (where the net reaction is H+Cl+allene/propyne). Thus, if the propyne photoionization efficiency curve redshifts significantly with increasing internal energy, we may not be able to assure that the vibrationally excited propyne product from HCl elimination would not be ionized at the 10 eV photoionization energy used to detect the products in Fig. 10. Nevertheless, the partial photoionization efficiency (PIE) curve showing signal from 80–100 μs, Fig. 8, for the allene/propyne products from HCl elimination that do not undergo secondary dissociation clearly shows a shoulder from allene photoionization. For the allene/propyne products not lost to secondary dissociation we can also attempt to determine the fraction of allene relative to the allene fraction determined for the near-threshold group of dissociating 2-propenyl radicals. The kinematically corrected ratio of relative contribution of allene+propyne from HCl elimination to the near threshold allene+propyne from 2-propenyl radical dissociation in Fig. 7 is 0.296, while the relative amount of allene/propyne from HCl elimination to allene from near-threshold radical dissociation at 10 eV photoionization (Fig. 10) is 2.25. Thus, if the 10 eV spectrum only detects allene from HCl elimination, the branching to allene from HCl elimination would be 7.6 times the branching to allene from the near-threshold dissociation of 2-propenyl radicals. Using 10.3% for the latter (as predicted from RRKM calculations) we might conclude that if the surviving mass 40 HCl products are representative of the nascent product branching, that 79% of the HCl eliminations form allene+HCl (6) and only 21% form propyne+HCl. However, the propyne formed in the HCl elimination channel is probably highly vibrationally excited, so it is dangerous to assume that the 10 eV photoionization would selectively detect the allene product. Indeed, our preliminary electronic structure calculations[30] on the two HCl elimination barriers suggest that if the HCl elimination proceeds by internal conversion, the propyne+HCl channel should be the dominant one. Thus the increased relative contribution from the shoulder resulting from the fast HCl elimination apparent in Fig. 10 probably reflects the fact that 10 eV photons can ionize both allene and propyne products from HCl elimination (since the propyne is highly vibrationally excited) but only allene products from 2-propenyl radical dissociation. Propyne product can also isomerize to allene if it has over 65 kcal/mol of internal energy, as much of the HCl elimination C_3H_4 products do. The small signal in the PIE spectrum in Fig. 9 below 9 eV is likely from the photoionization of highly vibrationally excited allene from HCl elimination, as it is most apparent in the PIE curve integrated over the arrival times of stable C_3H_4 product from HCl elimination.

3. Primary photodissociation product branching

The next section (Sec. III C 4) discusses a minor C–CH_3 fission channel identified as a primary photodissociation channel for 2-chloropropene excited at 193 nm. Assuming that the branching to that channel is small, we can derive a branching fraction for the direct C–Cl fission channel producing fast Cl atoms (hereafter ''fast C–Cl''), the C–Cl fission channel producing slow Cl atoms appearing with arrival times peaking near 150 μs in Fig. 4 (hereafter ''slow C–Cl''), and HCl elimination from 2-chloropropene (to produce allene or propyne). The fractional contribution from the fast C–Cl channel is obtained by adding together the two contributions to the fast peak in Fig. 4, one producing stable mass 41 product and one producing dissociative mass 41 product with near-threshold internal energy, as discussed above. The kinematically corrected ratio between the fast C–Cl channel and the slow C–Cl channel is derived directly from fitting the relative signals from each in Fig. 4. To obtain the relative contribution from HCl elimination, we need only assume that the vibrationally excited propyne/allene from the HCl elimination is detected as efficiently at 11 eV photoionization energy as the colder propyne/allene from the unimo-

lecular dissociation of the 2-propenyl radicals, and then use the kinematically corrected contributions to the fits of the mass 40 TOF spectrum in Fig. 7. Then the primary product branching, accounting for only the HCl elimination that produces propyne/allene stable to secondary dissociation, is: [fast C–Cl]:[slow C–Cl]:[HCl elimination producing stable products]=68%:26%:6%. If we account for all the HCl primary elimination events (accepting our estimate that 60% of the allene/propyne products from HCl elimination underwent secondary dissociation) then the primary product branching ratio is: [fast C–Cl]:[slow C–Cl]:[HCl elimination]=62%:23%:15%. These ratios of course assume that our detection sensitivity to propyne and allene are similar at 11 eV photoionization energy and that the sensitivity at 11 eV to vibrationally excited propyne/allene (from HCl elimination) stable to secondary dissociation is also similar to that for the colder C_3H_4 products from C–H fission in the 2-propenyl radical.

4. Methyl loss and subsequent secondary dissociation of the chlorovinyl radical

Fig. 16(A) shows the TOF spectrum collected at $m/e=61(C_2H_2Cl^+)$ at a source angle of 15° (photoionization energy=10.5 eV, 400 000 laser shots). The signal is momentum-matched to the signal at $m/e=15$ (CH_3^+, collected for 750 000 shots at 20°) shown in Fig. 16(B) so we assign these spectra to primary C–CH_3 bond fission in 2-chloropropene to form methyl+chlorovinyl radical. Figure 17 shows the primary C–CH_3 bond fission $P(E_T)$ used to fit the methyl and C_2H_2Cl data. Although the $m/e=15$ signal was collected for almost twice as many laser shots as the signal in Fig. 16, the signal-to-noise ratio remains poor due to the low-relative absorption cross section for the 10.5 eV photons used.[44] As discussed in the Introduction, secondary dissociation of C_2H_2Cl to C_2H_2+Cl (2) is energetically allowed. It is difficult to assess the amount of this secondary dissociation because the signal at $m/e=26$, $C_2H_2^+$, [Fig. 16(C)] clearly shows some signal that probably results from the $C_2H_2^+$ daughter ion from dissociative ionization of the chlorovinyl radical, C_2H_2Cl, from primary C–CH_3 fission. The fastest signal in the spectrum also appears at too fast an arrival time to be due to acetylene from the unimolecular decomposition of C_2H_2Cl from primary one-photon induced C–CH_3 bond fission in 2-chloropropene. Secondary dissociation of C_2H_2Cl into C_2HCl+H is also energetically allowed, but no significant signal was evident at $m/e=60$ after 440 000 laser shots.

IV. DISCUSSION

This discussion is organized in two parts. First, we focus on the competition between C–Cl bond fission, HCl elimination, and C–CH_3 fission of the 2-chloropropene and related molecules, and how that competition might evolve on the excited-state and ground-state potential energy surfaces of the molecule. Then we turn to the unimolecular dissociation channels of the 2-propenyl radicals, comparing our results with predictions of recent theoretical calculations of the C–H fission transition states for reactions (4) and (5) and with isomerization transition states to other C_3H_5 isomers.

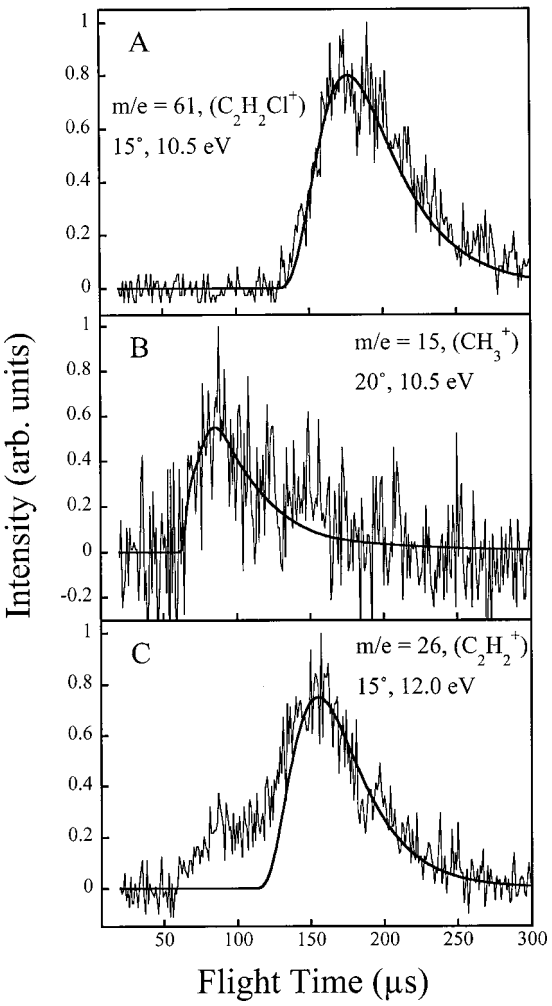

FIG. 16. (A) Time-of-flight spectrum of photofragments giving signal at $m/e=61$, $C_2H_2Cl^+$. (B) Time-of-flight spectrum of photofragments giving signal at $m/e=15$, CH_3^+. Fits shown in smooth solid line in (A) and (B) were calculated from the $P(E_T)$ for the C–CH_3 bond fission channel in 2-chloropropene shown in Fig. 17. (C) Time-of-flight spectrum of photofragments giving signal at $m/e=26$, $C_2H_2^+$ showing suggested contribution from dissociative ionization of the chlorovinyl radical, C_2H_2Cl, from primary C–CH_3 fission. The peak centered near 90 μs may be due, in part, to secondary unimolecular dissociation of C_2H_2Cl to Cl+acetylene, but the fastest signal in the spectrum appears at too fast an arrival time to be due to secondary acetylene products from the primary 1-photon C–CH_3 dissociation.

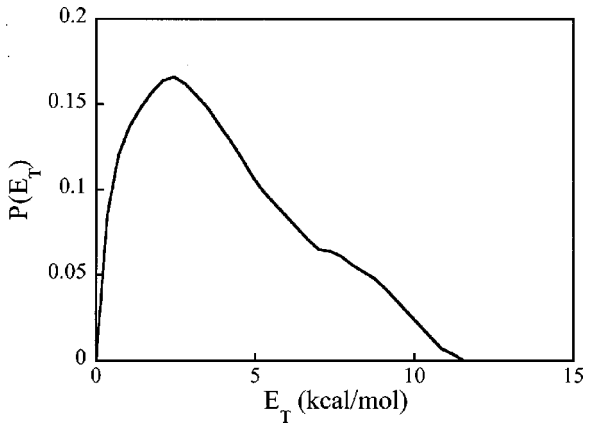

FIG. 17. Product kinetic-energy distribution, $P(E_T)$, for the C–CH_3 bond fission channel in 2-chloropropene derived from forward convolution fitting of Figs. 16(A) and 16(B).

We end by suggesting how the unimolecular dissociation pathways of the other straight-chain C_3H_5 radical isomers, allyl and 1-propenyl, might differ from those observed here for 2-propenyl radical and indicate the future directions of our ongoing experiments on these systems.

A. Primary photodissociation channels of 2-chloropropene at 193 nm

There are several interesting comparisons between the primary photofragmentation channels of 2-chloropropene excited at 193 nm and those of vinyl chloride[20–26] and allyl chloride[45] at the same wavelength. First, all three molecules evidence the ''fast C–Cl'' bond fission channel discussed here, while only vinyl chloride and 2-chloropropene, not allyl chloride, evidence significant branching to a photofragmentation channel producing slow Cl atoms. The C–Cl fission producing fast Cl atoms likely proceeds via a similar mechanism in all three molecules, predissociation of the nominal $\pi\pi^*$ excited state via a $n\sigma^*_{C-Cl}$ (or $\pi\sigma^*_{C-Cl}$ at nonplanar twisted geometries) repulsive state, which partitions considerable energy to product recoil translational energy. The distribution of energies partitioned to product translation for this fast C–Cl channel is very similar in vinyl chloride and 2-chloropropene, but is shifted to almost 20 kcal/mol higher recoil translational energies in allyl chloride. This may well be due to the significant[35] admixture of $n\sigma^*_{C-Cl}$ character in the $\pi\pi^*$ excited state in allyl chloride; that molecule feels a repulsive force acting to stretch the C–Cl bond even in the Franck–Condon region, thus partitioning more energy to product translation. The slow C–Cl fission channel is also much more minor in allyl chloride, contributing less than 3% of the total C–Cl fission.[45] It may be that repulsive forces in the Franck–Condon region of the excited state of allyl chloride act to stretch the C–Cl bond before the molecules have a chance to sample regions of the excited state from which they may undergo internal conversion to the ground-state potential-energy surface. The slow C–Cl fission channel in vinyl chloride was attributed to molecules that had undergone internal conversion to the ground electronic state before dissociation. This is also the likely mechanism for the slow C–Cl fission channel in 2-chloropropene. However, one consistency check is to compare the measured $P(E_T)$ for the slow C–Cl fission channel with a statistical distribution of energies to product translation predicted via RRKM theory. To calculate an RRKM $P(E_T)$, we arbitrarily chose a C–Cl bond distance of 2.5 Å on the ground-state reaction coordinate to locate a reasonable point to calculate frequencies at the ''transition state,'' optimizing the other bond lengths and angles at the MP2 level of theory. Figure 18 shows a comparison between this RRKM $P(E_T)$ and the measured $P(E_T)$ from Fig. 5 for the C–Cl bond fission we are attributing to dissociation of 2-chloropropene on the ground-state potential-energy surface. The comparison clearly supports the assignment of the slow C–Cl bond fission to a ground state mechanism. (We also used RRKM theory to estimate the probable branching to C–H fission (10) upon internal conversion because the work of Blank *et al.* on vinyl chloride detected primary C–H fission and attributed it to internal conversion. Because the barrier to C–H fission is much higher than the barrier to C–Cl fission, our RRKM rate constants for C–H fission[30] were a factor of 6.5 smaller than for C–Cl fission; detecting this small branching to C–H fission is made harder by the fact that most of such presumed statistical C–H fission events would partition less than 6.7 kcal/mol into product recoil. Three-center H_2 elimination is more likely to appear as a significant, though minor, dissociation channel, but it is expected to have a small exit barrier so is also unlikely to partition enough energy to product translation to be observable at the heavier photofragment in these experiments. The elimination/concerted isomerization mechanism that Blank *et al.*[23] invoke to explain the high-recoil kinetic energies for H_2 elimination in vinyl chloride is not possible in 2-chloropropene as there is no alpha H atom to migrate.)

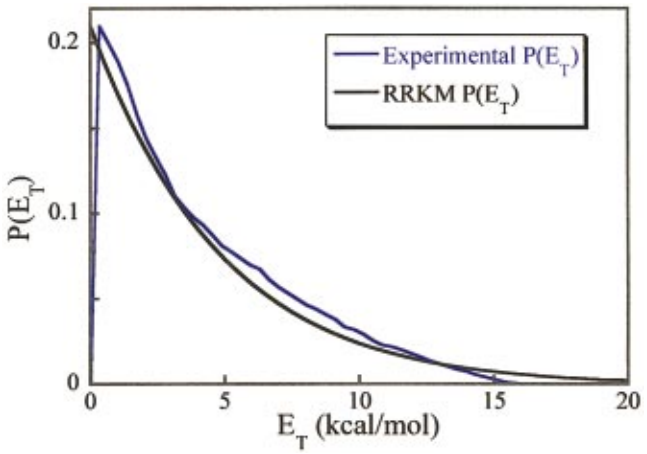

FIG. 18. (Color) Comparison between the experimental C–Cl fission $P(E_T)$ (from Fig. 5) measured for the slow Cl atoms with an RRKM predicted $P(E_T)$.

HCl elimination also occurs in all three molecules, but with marked differences. One might attribute HCl elimination in 2-chloropropene to reactions occurring after internal conversion to the ground electronic state, as proposed for vinyl chloride.[23,25] In contrast, in allyl chloride two distinct product kinetic-energy distributions were observed for HCl elimination, and the branching between those two channels showed a marked nozzle temperature dependence, suggesting at least one of them might occur via an excited-state elimination process.[45] Returning to the comparison between vinyl chloride and 2-chloropropene, the elimination in vinyl chloride was attributed to a 1,1-elimination with synchronous isomerization to acetylene to explain the high energies partitioned to product translation.[23,25] 2-chloropropene does not have a 1,1-elimination process available (there is a methyl rather than an H on the C–Cl carbon) so, of the two HCl elimination channels allowed for 2-chloropropene, only reaction (8), forming propyne, has an analog in vinyl chloride. It is analogous to the 1,2-elimination channel in vinyl chloride, which forms acetylene directly; this pathway was discounted in assigning the HCl elimination because *ab initio* calcula-

tions showed it had a higher barrier than 1,1-elimination. However, we note here that the measured $P(E_T)$ and the HCl PIE curves for HCl elimination in 2-chloropropene are remarkably similar to those in vinyl chloride, indicating a 1,2-elimination mechanism may dominate in both molecules. Although there is some evidence in the PIE spectrum for a contribution from the HCl elimination channel in 2-chloropropene which does not have an analog in vinyl chloride, it is likely that 1,2-elimination in 2-chloropropene is dominated by the HCl+propyne channel. We base this expectation on first assuming that HCl elimination proceeds via internal conversion and then predicting the rate constants for the two 1,2-elimination channels with RRKM theory[46] using calculated *ab initio* barriers and vibrational frequencies at each transition state. The zero-point-corrected *ab initio* barrier heights calculated by Parsons *et al.*[30] are nearly identical [74.2 kcal/mol for (6) and 73.3 kcal/mol for (8) at the MP2/6-311G(d,p) level of theory] and the molecule has over 147.9 kcal mol^{-1} of internal energy (see Fig. 1). Thus the ratio of our calculated[30] RRKM rate constants for the two channels, $k_8/k_6=1.7$ favoring propyne, results primarily from the fact that the HCl+propyne channel does not freeze the internal methyl rotor while the HCl+allene channel does, inducing a tighter transition state in reaction (6) than in reaction (8).

B. Competing C–H bond fission channels in the 2-propenyl radical unimolecular dissociation

The experiments presented here selectively resolved the product branching between the unimolecular dissociation channels of a high-energy C_3H_5 isomer, the 2-propenyl radical, measuring how the branching ratio between the two competing C–H fission channels changes as a function of internal energy. This is a unique capability that is easily extended to probing the internal energy dependence of the competition between unimolecular dissociation channels of a broad spectrum of hydrocarbon radicals that have eluded direct experimental probes in the past. Although the branching between the dissociation channels of the 2-propenyl radical as a function of internal energy has never been measured before, the system is small enough that high quality *ab initio* calculations[1,4] have been reported, adding to earlier[2,3,6] computational and empirical estimates of isomerization and dissociation barriers in the C_3H_5 systems, which allow us to predict the branching between product channels and how it changes with internal energy in the radical. We make that comparison below.

The experimental data showed the following. First, the fraction of 2-propenyl radicals that dissociate to give H+allene products is 2.0 ($+0.05/-0.15$) times larger for dissociation of the group of radicals with higher internal energy (median energy 15 kcal/mole above the barrier to H+propyne) than from the group of radicals with lower internal energy. Second, fitting the arrival times of allene derived from near-threshold 2-propenyl radicals showed that (i) the barrier to H+allene is higher than the barrier to H+propyne and (ii) the branching to the H+allene channel increases with internal energy above the H+allene barrier. In fact, we used the fitting of the near-threshold H+allene product channel in Fig. 10 to determine the internal energy required to surmount the barrier to H+propyne and the fitting of products from both internal energy groups to test whether the relative barrier heights predicted for the H+propyne and H+allene channels in recent G2(B3LYP) calculations[1] are consistent with our experimental results. We now describe the RRKM calculation used for this purpose and the results.

We used RRKM theory[30,46,47] to obtain both a quantitative prediction of how the branching between the H+allene and H+propyne channels changes as a function of internal energy in the 2-propenyl radical and to predict the shape of the $P(E_T)$ in red-dashed line in Fig. 11 that fit the near-threshold allene products and gave us a barrier for the H+allene product channel. We use the frequencies of the radical and transition state complexes and relevant moments of inertia[48] calculated by Davis, Law and Wang[1] to calculate RRKM rate constants for reactions (4) and (5). Their zero-point-corrected barrier to H+allene (4), 38.1 kcal mol^{-1}, is one kcal mol^{-1} higher than the barrier to H+propyne (5); see Fig. 1. (The barrier energy difference is in qualitative agreement with the 2 kcal/mol energy difference determined in the *ab initio* work of Deyerl *et al.*[4]). Thus we expect the group of dissociating 2-propenyl radicals with the lower internal energies to favor propyne products for barrier energy reasons alone. This expectation is borne out by fitting the 10 eV TOF spectrum, which reveals the internal energy dependence of the product branching even within the low-internal-energy group of dissociating radicals as shown in Figs. 10 and 11. To fit the time-of-arrival distribution of the near-threshold allene products, we already knew the number of dissociative radicals at each energy from momentum matching with the measured Cl atom TOF that are momentum-matched to the near-threshold 2-propenyl radicals. If these radicals branched between H+allene and H+propyne with a ratio independent of the internal energy of the radical, we could have fit the TOF of the allene products with the near-threshold (red) $P(E_T)$ in Fig. 5, but that gave a very poor fit. The data showed clearly that the onset of the H+allene channel was at higher internal energies (lower kinetic energies in Cl+C_3H_5 recoil) than H+propyne and that the branching to the H+allene channel increased with internal energy in the dissociating radical. Indeed, we used the RRKM calculations to predict the shape of the red-dashed line $P(E_T)$ in Fig. 11 that we used to fit the near-threshold allene products. We simply weighted the distribution of dissociative radicals at each energy with the RRKM prediction for what fraction of radicals at each internal energy would dissociate to H+allene instead of H+propyne, $k_{\text{allene}}(E^*)/(k_{\text{allene}}(E^*)+k_{\text{propyne}}(E'^*))$, where the available energy above the H+allene barrier (E^*) was, because of the 1 kcal/mol difference in barrier heights, 1 kcal/mol higher than E'^* for H+propyne. We originally assumed that the heats of formation of reactants and products, particularly 2-chloropropene, and the H+propyne/allene barrier heights with respect to the two product asymptotes were not accurate enough to derive an E^* corresponding to each kinetic energy for the RRKM predicted $P(E_T)$ in Fig. 11. Instead, we arbitrarily assigned a particular E_T in C–Cl fission as producing the radical with an $E'^*=0$ for the H+propyne channel, and calculated the RRKM rate con-

stants to generate a predicted $P(E_T)$ to fit the allene products in Fig. 10. Iterating this, we found that assigning $E_T = 17.4 \pm 2$ kcal/mol as producing 2-propenyl radical with $E^* = 0$ gave the red-dashed $P(E_T)$ in Fig. 11 that fit the near-threshold H+allene signal well. (with $E_T = 18.4 \pm -2$ kcal/mol giving $E'^* = 0$ for the H+propyne channel). This experimental determination is in remarkably good agreement with the prediction derived from computed heats of formation. Calculating the kinetic energy required to produce 2-propenyl radicals with an internal energy at the barrier to H+allene, we get

$$E_{T,\text{threshold,allene}} = E_{h\nu} + E_{\text{int,mp}} - \Delta H_{0\ K}(3+4) - E_{\text{exit barrier}}$$
$$= (147.9 + 1.2 - 128.4 - 3.1)\ \text{kcal/mol}$$
$$= 17.6 \pm 3.5\ \text{kcal/mol}.$$

This result corresponds closely to our experimental value of $E_{T,\text{threshold,allene}} = 17.4 \pm 2$ kcal/mol. The key number in the equation that could not be experimentally determined, and therefore, was only available from calculations, is the difference in energy between the barrier to H+allene and the asymptotic product energy. The barrier energy determined in the G3(B3LYP) calculations by Davis *et al.*[1] was 3.1 kcal/mole above the H+allene asymptote. Our threshold agrees with this to within 0.2 kcal/mol, well within the uncertainty in heats of formation used to make the comparison. (In contrast, if it were the allyl radical dissociating to H+allene, the barrier energy is predicted by Davis *et al.*[1] to be 5.6 kcal/mol higher than the H+allene asymptote.) Thus the excellent comparison with our experimental threshold supports the low 3.1 kcal/mol exit barrier (barrier to reverse reaction) for the 2-propenyl radical dissociation to H+allene. There are no other experimental determinations of this exit barrier, as no other experiment has been able to produce the 2-propenyl radical selectively and detect its branching to H+allene as a function of internal energy above the H+allene asymptote. (The other numbers used in the equation above are from thermodynamic measurements as follows. We assume that using in the equation above the most probable internal energy for the 2-chloropropene precursor, $E_{\text{int,mp}}$,1.2 kcal/mol at a nozzle temperature of 150 °C, which assumes no vibrational cooling in the expansion in He, gives us a reasonable way to estimate the kinetic energy at which the radicals are most likely to be formed with $E^* = 0$. To calculate the $\Delta H_{0\ K}$ for $H_2C{=}CClCH_3 \rightarrow H_2C{=}C{=}CH_2(\text{allene}) + H + Cl$ [(3) + (4)] we use literature[15] values for the heats of formation at 0 K for the Cl and the H and calculated values for 2-chloropropene[49] and allene.[50] Experimental heats of formation for 2-chloropropene[51] and allene[15] are only available at 298 K, so we use the G3 result at 0 K for 2-chloropropene of -1.3 ± 2.5 kcal/mol and the G3 result at 0 K for allene of 46.8 ± 2.5 kcal/mol. We should note that the literature values[52,53] for ΔH_f of the 2-propenyl radical yield values of ΔH_{rxn} for C–Cl bond fission in 2-chloropropene that gave predictions for the internal energy in the radical product that are inconsistent with the onset for secondary dissociation of the radical observed here. Therefore, we recommend instead using the calculated heats of formation above and the result from Davis *et al.*[1] that the zero-point energy of the 2-propenyl radical is 35 kcal/mol lower than the H+allene asymptote. This gives a derived heat of formation at 0 K of 63.4 kcal/mol for the 2-propenyl radical and a C–Cl bond energy in 2-chloropropene of 93.4 kcal/mol.)

The RRKM calculations using the transition states of Davis *et al.*[1] thus gave predictions in good agreement with our experimental results for both the exit barrier in the 2-propenyl radical→H+allene unimolecular dissociation (4) and for the change in branching between the H+propyne and H+allene channels as a function of internal energy from 0 to 18 kcal/mol above the H+propyne barrier. Experimentally we found that the quantum yield of allene from the higher internal energy group of radicals, with median internal energy 15 kcal/mol above the H+propyne barrier, is 2.0 $(+0.05/-0.15)$ times higher than the quantum yield of allene from the lower internal energy group of radicals. The RRKM calculations, appropriately averaged over the internal energy distributions for the two groups of radicals using the E^* and E'^* corresponding to each kinetic-energy release, adequately predict the observed change in branching, predicting a ratio of 2.2. Calibrating the experimental yield for the higher internal energy group of radicals with the RRKM yield predicted for the lower internal energy radicals, we find experimentally that only 21% of the 2-propenyl radicals with median internal energy 15 kcal/mol above the H+allene barrier give H+allene products. Note that the C–H fission product branching we resolve here from 2-propenyl radicals is very different than the dominance of H+allene products from allyl radical decomposition.[4,5] The rate of isomerization of 2-propenyl radical to allyl radical at the energies in our work must be small compared to the dissociation rates for 2-propenyl radicals; indeed there is considerable disagreement in the literature on the height of the isomerization barrier, some estimates[1,4] having the isomerization barrier higher than the 2-propenyl radical C–H bond fission barriers, and some[2,3,6,54] having it lower.

Figure 1 depicts a very interesting comparison offered by the (H+propyne)/(H+allene) product branching for the 2-propenyl radical dissociation and the HCl+propyne–HCl+allene product branching in HCl elimination from 2-chloropropene. Although the C–H fission reactions proceed through loose transition states and the HCl elimination through tight transition states, in both types of reactions the branching to the propyne products is predicted to be larger than the branching to allene products. The prediction persists even at very high excess energies above the barrier, so it cannot be attributed to the very small barrier energy differences for producing allene versus propyne. Thus any attempt to predict the preference for propyne formation based on relative barrier heights or endothermicities alone would not give the RRKM preference for propyne+H products at these higher internal energies. The preference for propyne formation over allene formation clearly results from the fact that propyne formation does not freeze an internal rotor at the

transition state in either the HCl elimination or the radical C–H fission reactions, while the rotor is frozen for allene formation in either type of reaction. The preference for the propyne products in these elimination and bond fission systems is thus a nice example of the general effect on rate constants of the tightening of the transition state when a methyl rotor is frozen. These experiments were only able to confirm the preference for propyne products in the 2-propenyl radical C–H fission reactions (the high vibrational excitation of the propyne product from the HCl elimination thwarted our attempt to determine the product isomer using tunable VUV photoionization). Work is underway in other labs regarding the HCl elimination channels in the thermal decomposition of 2-chloropropene.[55]

The experiments presented here open the door to studying the branching between unimolecular dissociation channels for selectively-produced hydrocarbon radical isomers as a function of internal energy in the radical isomer. Given the key role played by hydrocarbon radical isomers in combustion and atmospheric processes, a role embedded in kinetic mechanisms for such processes, the opportunities opened up here are very exciting. We are currently using the same method to compare the C–C and two C–H fission unimolecular decomposition channels of the allyl, 2-propenyl, and 1-propenyl C_3H_5 radical isomers and the corresponding unimolecular reactions of several key C_4H_7 radical isomers.

ACKNOWLEDGMENTS

This work was supported by the National Science Foundation under Grant Nos. CHE-9619376 and CHE-9974937 (L.J.B.) and by the Director, Office of Science, Office of Basic Energy Sciences, Chemical Sciences Division of the U.S. DOE, contract No. DE-AC03-76SF00098 (A.G.S.). The ALS is supported by the Materials Sciences Division of the DOE under the latter contract. J.M. gratefully acknowledges support from the Camille and Henry Dreyfus Foundation's Postdoctoral Program in Environmental Chemistry. The authors thank B. Ruscic for pursuing two key calculations of heats of formation that contributed to this work, Johanna Miller for carrying out the RRKM calculations and Bill Hase for helpful advice on them, and Congjun ''Panda'' Wang for aid in taking the UV-vis absorption spectrum. We also thank D. Neumark for donating the allene used to obtain the cold allene photoionization efficiency curve in this paper.

[1] Calculated in S. G. Davis, C. K. Law, and H. Wang, J. Phys. Chem. A **103**, 5889 (1999).
[2] J. Niedzielski, J. Gawlowski, and T. Gierczak, J. Photochem. **21**, 195 (1983).
[3] T. Gierczak, J. Gawlowski, and J. Niedzielski, J. Photochem. Photobiol., A **43**, 1 (1988).
[4] H-J. Deyerl, I. Fischer, and P. Chen, J. Chem. Phys. **110**, 1450 (1998).
[5] H.-J. Deyerl, T. Gilbert, I. Fischer, and P. Chen, J. Chem. Phys. **107**, 3329 (1997).
[6] D. Stranges, M. Stemmler, X. Yang, J. D. Chesko, A. G. Suits, and Y. T. Lee, J. Chem. Phys. **109**, 5372 (1998).
[7] H. Hunziker and H. H. Gunthard, Spectrochim. Acta **21**, 51 (1965).
[8] S. Bell, G. A. Guirgis, A. R. Fanning, and J. R. Durig, J. Mol. Struct. **178**, 63 (1988).
[9] L. H. London and K. D. Moller, J. Mol. Struct. **2**, 493 (1968).
[10] J.-F. Riehl and K. Morokuma, J. Chem. Phys. **100**, 8976 (1994).
[11] W. Tsang, in *Energetics of Organic Free Radicals*, edited by J. A. Simhoes, A. Greenberg, and J. F. Liebman (Blackie, London, 1996), p. 22.
[12] Assumes the C_2H_2 vinylidene radical product isomerizes on a time scale rapid compared to the dissociation process, so energy released in the isomerization is included in ΔH_{rxn}.
[13] Estimated from a ΔH_0 of 128.4 kcal/mol for $H_2C{=}CClCH_3 \rightarrow H_2C{=}C{=}CH_2$(allene)+H+Cl calculated as described in the Discussion and subtracting the endothermicity at 0 K of (4) calculated at the G2(B3LYP) level of theory in Ref. 1.
[14] Calculated from heats of formation at 0 K in Ref. 15 and a calculated heat of formation at 0 K at the G3 level of theory for 2-chloropropene by B. Ruscic referenced in the Discussion.
[15] H. M. Rosenstock, K. Draxl, B. W. Steiner, and J. T. Herron, J. Phys. Chem. Ref. Data Suppl. **6**, Suppl. 1, 774 (1977).
[16] A. M. Mebel, W. M. Jackson, A. H. H. Chang, and S. H. Lin, J. Am. Chem. Soc. **120**, 5751 (1998) but note that the allene-propyne zero-point energy level difference in this paper is 0.2 kcal/mol less than that given in Ref. 1.
[17] Calculated as described in Ref. 14 and subtracting the 1.1 kcal/mol zero-point energy level difference between allene and propyne reported in Ref. 1.
[18] Estimated by assuming they have similar endothermicities as the analogous reactions in vinyl chloride, cleavage of the *trans*-β C–H bond and H_2 elimination to form chlorovinylidene for the analogs to (8) and (10), respectively, calculated in Ref. 10.
[19] M. J. Berry, J. Chem. Phys. **61**, 3114 (1974).
[20] Y. Mo, K. Tonokura, Y. Matsumi *et al.*, J. Chem. Phys. **97**, 4815 (1992).
[21] M. Umemoto, K. Seki, H. Shinohara, U. Nagashima, N. Nishi, M. Kinoshita, and R. Shimada, J. Chem. Phys. **83**, 1657 (1985).
[22] P. T. A. Reilly, Y. Xie, and R. J. Gordon, Chem. Phys. Lett. **178**, 511 (1991).
[23] D. A. Blank, W. Sun, A. G. Suits, Y. T. Lee, S. W. North, and G. E. Hall, J. Chem. Phys. **108**, 5414 (1998).
[24] Y. Huang, Y.-A. Yang, G. He, and R. J. Gordon, J. Chem. Phys. **99**, 2752 (1993); Y. Huang, G. He, Y. Yang, S. Hashimoto, and R. J. Gordon, Chem. Phys. Lett. **229**, 621 (1994).
[25] Y. Huang, Y. Yang, G. He, S. Hashimoto, and R. J. Gordon, J. Chem. Phys. **103**, 5476 (1995).
[26] K. Tonokura, L. B. Daniels, T. Suzuki, and K. Yamashita, J. Phys. Chem. A **101**, 7754 (1997).
[27] M. Yoshimine, J. Pacansky, and N. Honjou, J. Am. Chem. Soc. **111**, 4198 (1989).
[28] J. H. Kiefer, S. S. Kumaran, and P. S. Mudipalli, Chem. Phys. Lett. **224**, 51 (1994).
[29] J. H. Kiefer, P. S. Mudipalli, S. S. Sidhu, R. D. Kern, B. S. Jursic, K. Xie, and H. Chen, J. Phys. Chem. A **101**, 4057 (1997).
[30] B. F. Parsons and L. J. Butler (in preparation).
[31] K. A. Holbrook, M. J. Pilling, and S. H. Robertson, *Unimolecular Reactions*, 2nd ed. (Wiley, New York, 1996), Chap. 3.
[32] X. Yang, J. Lin, Y. T. Lee, D. A. Blank, A. G. Suits, and A. M. Wodtke, Rev. Sci. Instrum. **68**, 3317 (1997).
[33] J. A. Mueller, J. L. Miller, L. J. Butler, F. Qi, O. Sorkhabi, and A. G. Suits, J. Phys. Chem. A. **104**, 11261 (2000).
[34] M. F. Arendt and L. J. Butler, J. Chem. Phys. **109**, 7835 (1998).
[35] P. W. Browning, D. C. Kitchen, M. F. Arendt, and L. J. Butler, J. Phys. Chem. **100**, 7765 (1996).
[36] B. F. Parsons, J. A. Mueller, S. L. Curry, P. C. Ray, and L. J. Butler, J. Chem. Phys. **111**, 8486 (1999).
[37] P. A. Heimann, M. Koike, C. W. Hsu *et al.*, Rev. Sci. Instrum. **68**, 1945 (1997).
[38] A. D. Walsh, Trans. Faraday Soc. **41**, 35 (1945).
[39] M. J. Frisch, G. W. Trucks, H. B. Schlegel *et al.* (Gaussian, Inc., Pittsburgh, PA., 1998).
[40] M. W. Schmidt, K. K. Baldridge, J. A. Boatz *et al.*, J. Comput. Chem. **14**, 1347 (1993).
[41] S. G. Lias, in *NIST Chemistry WebBook, NIST Standard Reference Database Number 69*, edited by W. G. Mallard and P. J. Linstrom, February 2000, National Institute of Standards and Technology, Gaithersburg MD, 20899 (http://webbook.nist.gov).
[42] W. Kuhnel, E. Gey, and B. Ondruschka, Z. Phys. Chem. (Leipzig) **268**, 23 (1987).

[43] S. G. Lias and J. F. Liebman, in *NIST Chemistry WebBook, NIST Standard Reference Database Number 69*, edited by W. G. Mallard and P. J. Linstrom, February 2000, National Institute of Standards and Technology, Gaithersburg MD, 20899 (http://webbook.nist.gov).
[44] W. A. Chupka and C. Lifshitz, J. Chem. Phys. **48**, 1109 (1968).
[45] T. L. Myers, D. C. Kitchen, B. Hu, and L. J. Butler, J. Chem. Phys. **104**, 5446 (1996); and the erratum **105**, 2948 (1996); M. L. Morton, T. A. Stephenson, F. Qi, and L. J. Butler (in preparation).
[46] K. A. Holbrook, M. J. Pilling, and S. H. Robertson, *Unimolecular Reactions*, 2nd ed. (Wiley, New York, 1996), Chap. 3.
[47] W. L. Hase, D. L. Bunker, A General RRKM Program, QCPE 234 (1974).
[48] The 59 cm^{-1} mode is replaced by a free rotor with $I=1.9$ amu $Å^2$, H. Wang (private communication).
[49] B. Ruscic, private communication of recent G3 calculations.
[50] B. Ruscic, private communication of recent G3 calculations.
[51] L. A. Shevtsova, A. M. Rozhov, and D. N. Andreevskii, Russ. J. Phys. Chem. **44**, 852 (1970) gives a value of -5.9 kcal/mol at 298 K.
[52] H. M. Rosenstock, K. Draxl, B. W. Steiner, and J. T. Herron, J. Phys. Chem. Ref. Data **6**, Suppl. 1, 774 (1977).
[53] J. L. Franklin and D. K. Sen Sharma, Adv. Mass Spectrom. **6**, 947 (1974).
[54] T. Ibuki, T. Murata, and Y. Takezaki, J. Phys. Chem. **78**, 2543 (1974).
[55] W. Tsang, private communication of work in progress.